

A Guidebook to Hunting Charged Higgs Bosons at the LHC

Abdesslam Arhrib ^{a,1}, Rachid Benbrik ^{b,c,2}, Hicham Harouiz ^{b,c,3} Stefano Moretti ^{d,4},
and Abdessamad Rouchad ^{b,c,5},

^a *Faculté des Sciences et Techniques, Abdelmalek Essaadi University, B.P. 416, Tangier, Morocco.*

^b *MSISM Team, Faculté Polydisciplinaire de Safi, Sidi Bouzid, B.P. 4162, Safi, Morocco.*

^c *LPHEA, Faculty of Science - Semlali, Cadi Ayyad University, P.O.B. 2390, Marrakech, Morocco.*

^d *School of Physics and Astronomy, University of Southampton, Southampton, SO17 1BJ, United Kingdom*

Abstract

We perform a comprehensive global analysis in the Minimal Supersymmetric Standard Model (MSSM) as well as in the 2-Higgs Doublet Model (2HDM) of the production and decay mechanisms of charged Higgs bosons (H^\pm) at the Large Hadron Collider (LHC). Starting from the most recent experimental results (SM-like Higgs boson signal strengths and search limits for new Higgs boson states obtained at Run-1 and -2 of the LHC and previous colliders), from (both direct and indirect) searches for Supersymmetric particles as well as from flavor observables (from both e^+e^- factories and hadron colliders) and upon enforcing theoretical constraints (vacuum stability, perturbativity, unitarity), we present precise predictions for H^\pm cross sections and decay rates in different reference scenarios of the two aforementioned models in terms of the parameter space currently available, specifically mapped over the customary $(m_{A,H^\pm}, \tan\beta)$ planes, including singling out specific Benchmark Points (BPs) amenable to phenomenological investigation. These include the $m_h^{\text{mod}+}$ and hMSSM configurations of the MSSM and the 2HDM Type-I, -II, -X and -Y. Such BPs are always close to (or coinciding with) the best fits of the theoretical scenarios to experimental data. We also briefly discuss the ensuing phenomenology for the purpose of aiding future searches for such charged Higgs boson states.

¹aarhrib@gmail.com

²r.benbrik@uca.ac.ma

³hicham.harouiz@edu.uca.ac.ma

⁴S.Moretti@soton.ac.uk

⁵abdessamad.rouchad@edu.uca.ac.ma

1 Introduction

The Higgs boson discovery of 2012 [1, 2, 3, 4] at the CERN Large Hadron Collider (LHC) has led to the confirmation of the Standard Model (SM) as the proper theory of the Electro-Weak (EW) scale. However, there is much evidence that the SM is not appropriate at all scales, rather it should be viewed as an effective low-energy realization of a more complete and fundamental theory onsetting beyond the EW regime. Among the many proposals for the latter, one can list theories with some new symmetry, e.g., Supersymmetry (SUSY), or an enlarged particle content (e.g., in the Higgs sector), or both. Following the aforementioned discovery, no new particle has however been seen at the LHC, implying that new physics at the EW scale should be weakly interacting or that strongly interacting particles, if present, should lead to signatures involving soft decay products or in channels with overwhelming (ir)reducible backgrounds. We shall adopt here the first assumption.

Many SM extensions possess in their spectra additional neutral and/or charged Higgs states. Amongst these, SUSY [5] is indeed considered the most appealing one as it addresses several shortcomings of the SM, including the problem of the large hierarchy between the EW and Planck scales. While the search for SUSY was unsuccessful during the first LHC run, the increase in the Center-of-Mass (CM) energy of the machine from 8 TeV to 13 TeV plus the additional luminosity of the second run are improving greatly the sensitivity to the new superparticles which are predicted. While the jury is still on these, we remind here the reader that SUSY also requires at least two Higgs doublets for a successful EW Symmetry Breaking (EWSB) pattern. For exactly two such fields, yielding the so-called Minimal Supersymmetry Standard Model (MSSM), also having the same gauge group structure of the SM, one obtains four physical Higgs particles, in addition to the discovered SM-like one with observed mass of 125 GeV. In fact, the same Higgs mass spectrum also belongs to a generic 2-Higgs Doublet Model (2HDM), i.e., one not originating from SUSY. In neither case, though, there exists a precise prediction of the typical masses of the new Higgs states, though we know already that the MSSM does not allow for any of these to be lighter than the 125 GeV one, whereas the 2HDM generally does [6, 7]. Either way, presence of extra physical Higgs boson states alongside the SM-like one is thus one of the characteristics of Beyond the SM (BSM) physics, whether within SUSY or otherwise. Hence, looking for these additional states in various production and decay channels over a wide range of kinematic regimes is an important part of the physics programme of the multi-purpose LHC experiments, ATLAS and CMS. Specifically, the discovery of a (singly) charged Higgs boson would point to a likely additional Higgs doublet. Hence, we concentrate on this Higgs state here.

The two Higgs doublet fields pertaining to the MSSM are required to break the EW symmetry and to generate the isospin-up and -down type fermions as well as the W^\pm and Z boson masses [8, 9, 10]. The Higgs spectrum herein is given by the following states: two charged H^\pm 's, a CP-odd A and two CP-even Higgses h and H , with $m_h < m_H$ (conventionally, wherein h is the SM-like Higgs state). The tree-level phenomenology of the Higgs sector of the MSSM is described entirely by two input parameters, one Higgs mass (that can be taken to be that of the CP-odd Higgs state, m_A) and the ratio $\tan\beta$ of the Vacuum Expectation Values (VEVs) of the two Higgs doublet fields. After the Higgs boson discovery at the LHC, MSSM benchmark scenarios have been refined to match the experimental data and to reveal characteristic features of certain regions of the parameter space [11, 12, 13]. Of the many MSSM frameworks presented in literature, we consider in this work the so-called $m_h^{\text{mod}+}$ [12] and hMSSM [14, 15] ones. The $m_h^{\text{mod}+}$ scenario is a modification of the time-honoured m_h^{max} scenario, which was originally defined to give conservative exclusion bounds on $\tan\beta$ in the context of Higgs boson searches at LEP, i.e., aimed at incorporating a rather light Higgs boson within the reach of the previous CERN machine. It has been eventually modified such that the mass of the lightest Higgs state, m_h , is compatible with the mass of the observed Higgs boson within ± 3 GeV in a large fraction of the considered parameter space. The hMSSM setup instead describes the MSSM Higgs sector in terms of just m_A and $\tan\beta$ given the experimental knowledge of m_Z and m_h . It defines a largely model-independent scenario, because the predictions of the properties of the MSSM Higgs bosons do not depend on the details of the Supersymmetric sector, somewhat unlike the previous case (wherein squark masses are fine-tuned to obtain $m_h \approx 125$ GeV).

As for the 2HDM, one ought to specify the Yukawa sector, in order to proceed to study phenomeno-

logically its manifestations. While SUSY enforces this in the form of a so-called Type-II, this is only one of four Ultra-Violet (UV) complete realizations of a generic 2HDM, the others been termed Type-I, -X and -Y. The difference between these four scenarios is the way the fermionic masses are generated. We define as Type-I the model where only one doublet couples to all fermions, Type-II is the scenario where one doublet couples to up-type quarks and the other to down-type quarks and leptons, the Type-X is the model where one doublet couples to all quarks and the other to all leptons while a Type-Y is built such that one doublet couples to up-type quarks and to leptons and the other to down-type quarks. In all such cases, the number of free parameters at tree-level is seven to start with, hence it becomes more cumbersome than in SUSY to map experimental results onto theoretical constraints. Yet, in virtue of the fact that a 2HDM is the simplest realization of a BSM scenario based solely on doublet Higgs fields, its study is vigorously being pursued experimentally.

So far, the non-observation of any Higgs signal events in direct searches above and beyond those of the SM-like Higgs state constrain the parameter space of the underlying physics model. Specifically, in the case of the H^\pm boson, wherein the relevant phenomenological parameters are m_{H^\pm} and $\tan\beta$ in whatever scenario, one can pursue the study of its production and decay modes in a model independent way, which results can a posteriori be translated to exclude the relevant parameter space in a given scenario (whether it be the MSSM, 2HDM or something else). This recasting is conveniently done on the $(m_A, \tan\beta)$ and $(m_{H^\pm}, \tan\beta)$ planes for the MSSM and 2HDM, respectively, so that we will map our findings in the same way.

At hadron colliders, there exists many production modes for charged Higgs bosons which are rather similar in the MSSM and 2HDM. For a light charged Higgs, i.e., with mass $m_{H^\pm} + m_b < m_t$, its production comes mainly from top decay. At the LHC, the production of top quark pairs proceeds via Quantum Chromo-Dynamics (QCD) interactions and, when kinematically allowed, one top could decay into a charged Higgs state and a bottom quark in a competition with the SM decay into a W^\pm boson and again a bottom quark. Therefore, the complete H^\pm production mechanism $q\bar{q}, gg \rightarrow t\bar{t} \rightarrow t\bar{b}H^\pm$ provides the main source of light charged Higgs bosons at the LHC and offers a much more copious signature than any other form of direct production. After crossing the top-bottom threshold, i.e., when $m_{H^\pm} + m_b > m_t$, a charged Higgs (pseudo)scalar can be produced through the process $gb \rightarrow tH^\pm$ [16, 17]. In fact, these two mechanisms can be simultaneously captured via the process $gg \rightarrow t\bar{b}H^\pm$ [18], which again makes it clear that one should expect large H^\pm cross sections induced by QCD interactions also in the heavy H^\pm mass range⁶.

In the MSSM, and also in a variety of 2HDM Types, light charged Higgs bosons would decay almost exclusively into a (hadronic or leptonic) τ lepton and its associated neutrino for $\tan\beta \gtrsim 1$. When the top-bottom channel is kinematically open, then $H^+ \rightarrow t\bar{b}$ would compete with $H^\pm \rightarrow hW^\pm, HW^\pm, AW^\pm$ decays as well as various SUSY channels in the MSSM. In the latter, $H^+ \rightarrow t\bar{b} \rightarrow b\bar{b}W^+$ is the dominant channel and the bosonic decays $H^\pm \rightarrow hW^\pm, HW^\pm, AW^\pm$ (also yielding $b\bar{b}W^+$ final states) are subleading. In the 2HDM, if none of these bosonic decays is open, then $H^+ \rightarrow t\bar{b}$ is the dominant mode. At the LHC Run-1, lighter charged Higgs bosons were probed in the decay channels $\tau\nu$ [19, 20], cs [21, 22] and also cb [23]. No excess was observed and model independent limits are set on the following product of Branching Ratios (BRs): $\text{BR}(t \rightarrow H^+b) \times \text{BR}(H^+ \rightarrow \tau\nu)$. At Run-2, mainly the decay modes $\tau\nu$ [24, 25] and tb [26] are explored in the mass range $m_{H^\pm} = 200$ GeV to 1000 GeV, in the latter mode using multi-jet final states with one electron or muon from the top quark decay. No significant excess above the background-only hypothesis has been observed and upper limits are set on the $pp \rightarrow t\bar{b}H^\pm$ production cross section times $\text{BR}(H^\pm \rightarrow tb)$. Several interpretations of these limits have eventually been given in benchmark scenarios of the MSSM, including those mentioned above. Note that current ATLAS and CMS bounds are significantly weakened in the 2HDM once the exotic decay channels into a lighter neutral Higgs, $H^\pm \rightarrow hW^\pm$ or $H^\pm \rightarrow AW^\pm$, are open. This scenario could also happen in the MSSM if one of the SUSY decay channels of charged Higgs bosons are open (such as into chargino-neutralino pairs). In the 2HDM, the possibility of producing a light charged Higgs boson from top decay with a subsequent step $H^\pm \rightarrow hW^\pm$ or $H^\pm \rightarrow AW^\pm$ was studied in [27] and it was shown that it can lead to

⁶For a complete review on charged Higgs production modes, see [17].

sizable cross sections at low $\tan\beta$.

In this paper, we analyze the allowed $\sigma(pp \rightarrow t\bar{b}H^\pm + \text{c.c.}) \times \text{BR}(H^\pm \rightarrow \text{anything})$ rates by taking into account both theoretical and experimental constraints on the underlying BSM model, the latter including the latest ATLAS and CMS results for SM-Higgs (h) and other Higgs (H, A, H^\pm) searches with the full set of 36.5 fb^{-1} data collected to date in the second LHC phase. We will then interpret these results under the proposed scenarios to quantify the magnitude of the available parameter space to be covered by future LHC analyses. In doing so, we will extract several Benchmark Points (BPs) that could lead to detectable signals, all of which are consistent with the best fit regions in both the MSSM and the 2HDM.

The paper is organized as follows. In the second section we review the MSSM and the 2HDM. The third section is devoted to a discussion of the theoretical and experimental constraints used in our study. Results and conclusions follow suit.

2 The MSSM

In the MSSM, due to the holomorphy of the Superpotential, one introduces two Higgs doublets $\phi_{1,2}$ in order to give masses to up-type quarks, down-type quarks and leptons. Both Higgs fields acquire VEVs $v_{1,2}$. After EWSB takes place, the spectrum of the model contains the aforementioned Higgs states: h, H, A and H^\pm . The MSSM Higgs sector is parameterized at tree-level by $\tan\beta = v_2/v_1$ and, e.g., the CP-odd mass m_A ⁷, while the top quark mass and the associated squark masses and their soft SUSY breaking parameters enter through radiative corrections [28, 29, 30].

To compute the masses and the couplings of Higgs bosons in a given point of the MSSM parameter space we use the public code FeynHiggs [31, 32], which includes the full one-loop and a large part of the dominant two-loop corrections to the neutral Higgs masses. Since the theoretical uncertainty on the Higgs mass calculation in the FeynHiggs code has been estimated to be of the order of 3 GeV, we consider as phenomenologically acceptable the points in the MSSM parameter space where FeynHiggs predicts the existence of a scalar with mass between 122.5 GeV and 128.5 GeV and with approximately SM-like couplings to gauge bosons and fermions. In addition to the tree-level scalar potential parameters, $\tan\beta$ and m_A , when taking into account high order corrections, the MSSM parameters most relevant to the prediction of the masses and production cross sections of the Higgs bosons are: the soft SUSY-breaking masses for the stop and sbottom squarks, which, for simplicity, we assume all equal to a common mass parameter M_S , the soft SUSY-breaking gluino mass $m_{\tilde{g}}$, the soft SUSY-breaking Higgs-squark-squark couplings A_t and A_b , the Superpotential Higgs-mass parameter μ and the left-right mixing terms in the stop and sbottom mass matrices

$$X_t = A_t - \mu \cot\beta, \quad X_b = A_b - \mu \tan\beta, \quad (1)$$

respectively. Since the two-loop calculation of the Higgs masses implemented in FeynHiggs and the Next-to-Leading Order (NLO) calculation of QCD corrections to the production cross section implemented in SusHi [33, 34] employ the same renormalization (on-shell) scheme, the input values of the soft SUSY-breaking parameters can be passed seamlessly from the Higgs mass to the cross section calculations.

A detailed description of the two benchmark scenarios adopted in our analysis, i.e., $m_h^{\text{mod}+}$ and hMSSM, can be found in [12]. Both are characterized by relatively large values of the ratio X_t/M_S , ensuring that the mass of the SM-like Higgs state falls within the required range without the need for an extremely heavy stop. In addition, the masses of the gluino and first two generation squarks are set to 1.5 TeV, large enough to evade the current ATLAS and CMS limits stemming from SUSY searches [35, 36, 37, 38, 39]. We vary the parameters $\tan\beta$ and m_A within the following ranges:

$$0.5 \leq \tan\beta \leq 15, \quad 90 \text{ GeV} \leq m_A \leq 1 \text{ TeV}. \quad (2)$$

The soft trilinear term A_t is set to be equal to A_b . Due to the smallness of the light quark masses, the left-right mixing of the first two generation squarks is neglected. The gaugino mass parameters M_1, M_2

⁷Notice that, in the light of the latest LHC data on the discovered Higgs boson, in the MSSM, the A and H^\pm states are essentially degenerate in mass.

and the soft SUSY-breaking gluino mass $m_{\tilde{g}}$ are all related through Renormalization Group Equation (RGE) running to some common high scale $m_{1/2}$ soft term which yields the relations $m_{\tilde{g}} \approx 3.5M_2$ and $M_1 \approx 0.5M_2$. In our analysis, we assume Grand Unified Theory (GUT) relations only between M_1 and M_2 while M_2 and $m_{\tilde{g}}$ are taken independent from each other. Finally, the soft SUSY-breaking parameters in the slepton sector have a very small impact on the predictions for the Higgs masses and production cross sections, therefore we do not report on them here.

3 The 2HDM

In this section, we define the scalar potential and the Yukawa sector of the general 2HDM. The most general scalar potential which is $SU(2)_L \otimes U(1)_Y$ invariant is given by [40, 41]

$$\begin{aligned}
V(\Phi_1, \Phi_2) &= m_1^2 \Phi_1^\dagger \Phi_1 + m_2^2 \Phi_2^\dagger \Phi_2 - (m_{12}^2 \Phi_1^\dagger \Phi_2 + \text{h.c.}) + \frac{1}{2} \lambda_1 (\Phi_1^\dagger \Phi_1)^2 \\
&+ \frac{1}{2} \lambda_2 (\Phi_2^\dagger \Phi_2)^2 + \lambda_3 (\Phi_1^\dagger \Phi_1) (\Phi_2^\dagger \Phi_2) + \lambda_4 (\Phi_1^\dagger \Phi_2) (\Phi_1^\dagger \Phi_2) \\
&+ \left[\frac{\lambda_5}{2} (\Phi_1^\dagger \Phi_2)^2 + \text{h.c.} \right].
\end{aligned} \tag{3}$$

The complex (pseudo)scalar doublets Φ_i ($i = 1, 2$) can be parameterized as

$$\Phi_i(x) = \begin{pmatrix} \phi_i^+(x) \\ \frac{1}{\sqrt{2}} [v_i + \rho_i(x) + i\eta_i(x)] \end{pmatrix}, \tag{4}$$

with $v_{1,2} \geq 0$ being the VEVs satisfying $v = \sqrt{v_1^2 + v_2^2}$, with $v = 246.22$ GeV. Hermiticity of the potential forces $\lambda_{1,2,3,4}$ to be real while λ_5 and m_{12}^2 can be complex. In this work we choose to work in a CP-conserving potential where both VEVs are real and so are also λ_5 and m_{12}^2 .

After EWSB, three of the eight degrees of freedom in the Higgs sector of the 2HDM are eaten by the Goldstone bosons (G^\pm and G) to give masses to the longitudinal gauge bosons (W^\pm and Z). The remaining five degrees of freedom becomes the aforementioned physical Higgs bosons. After using the minimization conditions for the potential together with the W^\pm boson mass requirement, we end up with seven independent parameters which will be taken as

$$m_h, m_H, m_A, m_{H^\pm}, \alpha, \tan \beta, m_{12}^2, \tag{5}$$

where, as usual, $\tan \beta \equiv v_2/v_1$ and β is also the angle that diagonalizes the mass matrices of both the CP-odd and charged Higgs sector while the angle α does so in the CP-even Higgs sector.

The most commonly used version of a CP-conserving 2HDM is the one which satisfy a discrete Z_2 symmetry $\Phi_i \rightarrow (-1)^{i+1} \Phi_i$ ($i = 1, 2$), that, when extended to the Yukawa sector, guarantees the absence of Flavor Changing Neutral Currents (FCNCs). Such a symmetry would also require $m_{12}^2 = 0$, unless we tolerate a soft violation of this by the dimension two term m_{12}^2 (as we do here). The Yukawa Lagrangian can then be written as

$$-\mathcal{L}_Y = \bar{Q}_L (Y_1^d \Phi_1 + Y_2^d \Phi_2) d_R + \bar{Q}_L (Y_1^u \tilde{\Phi}_1 + Y_2^u \tilde{\Phi}_2) u_R + \bar{L}_L (Y_1^l \Phi_1 + Y_2^l \Phi_2) l_R + \text{h.c.}, \tag{6}$$

where $Q_L^T = (u_L, d_L)$ and $L_L^T = (l_L, l_L)$ are the left-handed quark doublet and lepton doublet, respectively, the Y_k^f 's ($k = 1, 2$ and $f = u, d, l$) denote the 3×3 Yukawa matrices and $\tilde{\Phi}_k = i\sigma_2 \Phi_k^*$ ($k = 1, 2$). Since the mass matrices of the quarks and leptons are a linear combination of Y_1^f and Y_2^f , $Y_{1,2}^{d,l}$ and $Y_{1,2}^u$ cannot be diagonalized simultaneously in general. Therefore, neutral Higgs Yukawa couplings with flavor violation appear at tree-level and contribute significantly to FCNC processes such as $\Delta M_{K,B,D}$ as well as $B_{d,s} \rightarrow \mu^+ \mu^-$ mediated by neutral Higgs exchanges. To avoid having those large FCNC processes, one known solution is to extend the Z_2 symmetry to the Yukawa sector. When doing so, we end up with the already discussed four possibilities regarding the Higgs bosons couplings to fermions [41].

	κ_u^h	κ_d^h	κ_l^h	κ_u^H	κ_d^H	κ_l^H	κ_u^A	κ_d^A	κ_l^A
Type-I	c_α/s_β	c_α/s_β	c_α/s_β	s_α/s_β	s_α/s_β	s_α/s_β	c_β/s_β	$-c_\beta/s_\beta$	$-c_\beta/s_\beta$
Type-II	c_α/s_β	$-s_\alpha/c_\beta$	$-s_\alpha/c_\beta$	s_α/s_β	c_α/c_β	c_α/c_β	c_β/s_β	s_β/c_β	s_β/c_β
Type-X	c_α/s_β	c_α/s_β	$-s_\alpha/c_\beta$	s_α/s_β	s_α/s_β	c_α/c_β	c_β/s_β	$-c_\beta/s_\beta$	s_β/c_β
Type-Y	c_α/s_β	$-s_\alpha/c_\beta$	c_α/s_β	s_α/s_β	c_α/c_β	s_α/s_β	c_β/s_β	s_β/c_β	$-c_\beta/s_\beta$

Table 1: Yukawa couplings in terms of mixing angles in the four 2HDM Types.

After EWSB, the Yukawa Lagrangian can be expressed in the mass eigenstate basis as follows [42, 43]:

$$\begin{aligned}
\mathcal{L}_Y = & - \sum_{f=u,d,\ell} \frac{m_f}{v} \left(\xi_h^f \bar{f} f h + \xi_H^f \bar{f} f H - i \xi_A^f \bar{f} \gamma_5 f A \right) \\
& - \left(\frac{\sqrt{2} V_{ud}}{v} \bar{u} (m_u \xi_A^u P_L + m_d \xi_A^d P_R) d H^+ + \text{h.c.} \right). \tag{7}
\end{aligned}$$

We give in Tab. 1, the values of the Yukawa couplings in the four 2HDM Types. The couplings of h and H to gauge bosons $V = W^\pm, Z$ are proportional to $\sin(\beta - \alpha)$ and $\cos(\beta - \alpha)$, respectively. Since these are gauge couplings, they are the same for all Yukawa types. As we are considering the scenario where the lightest neutral Higgs state is the 125 GeV scalar, the SM-like Higgs boson h is recovered when $\cos(\beta - \alpha) \approx 0$. As one can see from Tab. 1, for all 2HDM Types, this is also the limit where the Yukawa couplings of the discovered Higgs boson become SM-like. The limit $\cos(\beta - \alpha) \approx 0$ seems to be favored by LHC data, except for the possibility of a wrong sign limit [44, 45], where the couplings to down-type quarks can have a relative sign to the gauge bosons ones, thus oppositely to those of the SM. Our benchmarks will focus on the SM-like limit where indeed $\cos(\beta - \alpha) \approx 0$.

We end this section by noticing that we have used the public program 2HDMC [46] to evaluate the 2HDM spectrum as well as the decay rates and BRs of all Higgs particles.

4 Theoretical and experimental constraints

In order to perform a systematic scan over the parameter space of the two MSSM configurations and the four 2HDM Types, we take into account the following theoretical⁸ and experimental constraints.

4.1 Theoretical constraints

We list these here as itemised entries.

- **Vacuum stability** To ensure that the scalar potential is bounded from below, it is enough to assume that the quartic couplings should satisfy the following relations [47]:

$$\lambda_{1,2} > 0, \quad \lambda_3 > -(\lambda_1 \lambda_2)^{1/2} \quad \text{and} \quad \lambda_3 + \lambda_4 - |\lambda_5| > -(\lambda_1 \lambda_2)^{1/2}. \tag{8}$$

We also impose that the potential has a minimum that is compatible with EWSB. If this minimum is CP-conserving, any other possible charged or CP-violating stationary points will be a saddle point above the minimum [48]. However, there is still the possibility of having two coexisting CP-conserving minima. In order to force the minimum compatible with EWSB, one need to impose the following simple condition [49]:

$$m_{12}^2 \left(m_{11}^2 - m_{22}^2 \sqrt{\lambda_1/\lambda_2} \right) \left(\tan \beta - \sqrt[4]{\lambda_1/\lambda_2} \right) > 0. \tag{9}$$

⁸Notice that, for the MSSM scenarios considered here, the (dynamically generated) scalar potential is stable in vacuum and does not induce perturbative unitarity violations.

Writing the minimum conditions as

$$\begin{aligned} m_{11}^2 + \frac{\lambda_1 v_1^2}{2} + \frac{\lambda_3 v_2^2}{2} &= \frac{v_2}{v_1} \left[m_{12}^2 - (\lambda_4 + \lambda_5) \frac{v_1 v_2}{2} \right], \\ m_{22}^2 + \frac{\lambda_2 v_2^2}{2} + \frac{\lambda_3 v_1^2}{2} &= \frac{v_1}{v_2} \left[m_{12}^2 - (\lambda_4 + \lambda_5) \frac{v_1 v_2}{2} \right], \end{aligned} \quad (10)$$

allows us to express m_{11}^2 and m_{22}^2 in terms of the soft Z_2 breaking term m_{12}^2 and the quartic couplings λ_{1-5} .

- **Perturbative unitarity** Another important theoretical constraint on the (pseudo)scalar sector of the 2HDM is the perturbative unitarity requirement. We require that the S -wave component of the various (pseudo)scalar scattering amplitudes of Goldstone and Higgs states remain unitary. Such a condition implies a set of constraints that have to be fulfilled and are given by [50]

$$|a_{\pm}|, |b_{\pm}|, |c_{\pm}|, |f_{\pm}|, |e_{1,2}|, |f_1|, |p_1| < 8\pi, \quad (11)$$

where

$$\begin{aligned} a_{\pm} &= \frac{3}{2}(\lambda_1 + \lambda_2) \pm \sqrt{\frac{9}{4}(\lambda_1 - \lambda_2)^2 + (2\lambda_3 + \lambda_4)^2}, \\ b_{\pm} &= \frac{1}{2}(\lambda_1 + \lambda_2) \pm \frac{1}{2}\sqrt{(\lambda_1 - \lambda_2)^2 + 4\lambda_4^2}, \\ c_{\pm} &= \frac{1}{2}(\lambda_1 + \lambda_2) \pm \frac{1}{2}\sqrt{(\lambda_1 - \lambda_2)^2 + 4\lambda_5^2}, \\ e_1 &= \lambda_3 + 2\lambda_4 - 3\lambda_5, & e_2 &= \lambda_3 - \lambda_5, \\ f_+ &= \lambda_3 + 2\lambda_4 + 3\lambda_5, & f_- &= \lambda_3 + \lambda_5, \\ f_1 &= \lambda_3 + \lambda_4, & p_1 &= \lambda_3 - \lambda_4. \end{aligned} \quad (12)$$

- **EW Precision Observables (EWPOs)** The additional neutral and charged (pseudo)scalars, beyond the SM-like Higgs state, contribute to the gauge bosons vacuum polarization through their coupling to gauge bosons. In particular, the universal parameters S , T and U provide constraints on the mass splitting between the heavy states m_H , $m_{H\pm}$ and m_A in the scenario in which h is identified with the SM-like Higgs state. The general expressions for the parameters S , T and U in 2HDMs can be found in [51]. To derive constraints on the scalar spectrum we consider the following values for S , T and U :

$$\Delta S = 0.05 \pm 0.11, \quad \Delta T = 0.09 \pm 0.13, \quad \Delta U = 0.01 \pm 0.11, \quad (13)$$

while using the corresponding covariance matrix given in [52]. The χ^2 function is then expressed as

$$\chi^2 = \sum_{i,j} (X_i - X_i^{\text{SM}})(\sigma^2)_{ij}^{-1}(X_j - X_j^{\text{SM}}), \quad (14)$$

with correlation factor +0.91.

The aforementioned 2HDMC program also allows us to check all the above theoretical constraints such as perturbative unitarity, boundedness from below of the scalar potential as well as EWPOs (S , T and U), which are all turned on during the calculation, and can be adapted to the MSSM as well.

4.2 Experimental constraints

The parameter space of our benchmark scenarios is already partially constrained by the limits obtained from various searches for additional Higgs bosons at the LHC as well as the requirement that one of the

neutral scalar states should match the properties of the observed SM-like Higgs boson. We evaluate the former constraints with the code HiggsBounds [53, 54, 55, 56] and the latter with the code HiggsSignals [57]. We stress, however, that our study of the existing constraints cannot truly replace a dedicated analysis of the proposed benchmark scenarios by ATLAS and CMS, which alone would be able to combine the results of different searches taking into account all correlations. In this section we briefly summarize the relevant features of HiggsBounds and HiggsSignals used in our study.

4.2.1 Collider constraints

The code HiggsBounds tests each parameter point for 95% Confidence Level (CL) exclusion from Higgs searches at the LHC as well as LEP and Tevatron. First, the code determines the most sensitive experimental search available, as judged by the expected limit, for each additional Higgs boson in the model. Then, only the selected channels are applied to the model, i.e., the predicted signal rate for the most sensitive search of each additional Higgs boson is compared to the observed upper limit. In the case the prediction exceeds the limit, the parameter point is regarded as excluded. For more details on the procedure, the reader can see Ref. [56].

Among the searches that are relevant in constraining our scenarios for charged Higgs studies, the latest version, 5.2.0beta, of HiggsBounds includes the following.

- ATLAS [58] and CMS [59] searches for heavy Higgs bosons decaying to $\tau^+\tau^-$ pairs using about 36 fb^{-1} of Run-2 data as well as the CMS results from Run 1 [60].
- Searches at Run-1 and Run-2 by ATLAS [61, 62] and CMS [63, 64] for a heavy scalar decaying to a Z boson pair, $H \rightarrow ZZ$.
- Searches at Run-1 and Run-2 by ATLAS [65] and CMS [66, 67] for a heavy scalar decaying to a pair of 125 GeV SM-like Higgs scalars, $H \rightarrow hh$.
- Searches at Run-1 by ATLAS [68] and CMS [69] for the 125 GeV scalar decaying to a pair of lighter pseudoscalars, $h \rightarrow AA$.
- Searches at Run-1 by ATLAS [70] and CMS [71] for a heavy pseudoscalar decaying to a Z boson and the 125 GeV scalar, $A \rightarrow Zh$.

By comparing these results with the predictions of SusHi, FeynHiggs and 2HDMC for the production cross sections and decay BRs of the additional neutral Higgs bosons, HiggsBounds reconstructs the 95% CL exclusion contours for our benchmark scenarios. In the MSSM and 2HDM Type II, these constraints are typically stronger for large values of $\tan\beta$, due to an enhancement of the production cross section of the heavier Higgs bosons in bottom-quark annihilation (in that case the most relevant searches are those for the decay to a $\tau^+\tau^-$ pair).

HiggsBounds also contains the available constraints from searches for a charged Higgs boson by ATLAS and CMS. Most relevant in our scenarios are the constraints on the production of a light charged Higgs via top quark decay, $t \rightarrow H^+b$, with subsequent decay $H^+ \rightarrow \tau^+\nu$ [19, 20, 25, 72], as well as top-quark associated H^\pm production, with subsequent decays to the $\tau\nu$ [19, 20, 25, 72] and/or tb [20, 26, 73] channels.

In order to estimate the theoretical uncertainty in our determination of the excluded regions, we rely on the uncertainty estimates for the gluon-fusion and bottom-quark annihilation cross sections. The most conservative (i.e., weakest) determination of the exclusion region is obtained by taking simultaneously the lowest values in the uncertainty range for both production processes of each of the heavier Higgs bosons, while the least conservative (i.e., strongest) determination is obtained by taking simultaneously the highest values in the uncertainty range.

With the use of the code HiggsSignals, we test the compatibility of our scenarios with the observed SM-like Higgs signals, by comparing the predictions of SusHi, FeynHiggs and 2HDMC for the signal strengths of Higgs production and decay in a variety of channels against the measurements by ATLAS

and CMS. The latest version, 2.2.0beta, of HiggsSignals includes all the combined ATLAS and CMS results from Run-1 of the LHC [74] as well as all the available ATLAS [75, 76, 77, 78, 79, 80, 81] and CMS limits [82, 83, 84, 85, 86, 87, 88, 89, 90] from Run-2.

4.3 Numerical results

In this subsection, we present our findings for the MSSM and 2HDM in turn.

4.4 MSSM results

In the hMSSM scenario, all Superparticles are chosen to be rather heavy so that production and decays of the MSSM Higgs bosons are only mildly affected by their presence due to decoupling properties of SUSY. In particular, the loop-induced SUSY contributions to the couplings of the light CP-even scalars are small and the heavy Higgs bosons with masses even up to 2 TeV decay only to SM particles. Therefore, the phenomenology of this scenario at the LHC resembles that of a 2HDM Type-II with MSSM-inspired Higgs couplings and mass relations. The SUSY input parameters are fixed as

$$\begin{aligned}
 M_{Q_3} = M_{U_3} = M_{D_3} = 1.5 \text{ TeV}, \quad M_{L_3} = M_{E_3} = 2 \text{ TeV}, \\
 \mu = 200 \text{ GeV}, \quad M_1 = 1 \text{ TeV}, \quad M_2 = 200 \text{ TeV}, \quad M_3 = 1.5 \text{ TeV}, \\
 X_t = 2M_{\text{SUSY}} = 2\text{TeV}, \quad A_b = A_\tau = A_t,
 \end{aligned}
 \tag{15}$$

where M_{SUSY} is the SUSY mass scale (essentially M_S).

The masses of the third generation squarks and that of the gluino are safely above the current bounds from direct searches at the LHC, as intimated. Specifically, we refer to [91, 92, 93, 94, 95, 96, 97, 98] for the scalar top quarks, [91, 92, 99, 100, 101] for the scalar bottom quarks and [92, 100, 102, 103, 104] for the gluino. The value chosen for X_t is close to the one for which the maximal value of m_h is obtained. The $m_h^{\text{mod+}}$ scenario is very similar to the hMSSM one except the fact that we take $X_t = 2M_{\text{SUSY}} = 1 \text{ TeV}$.

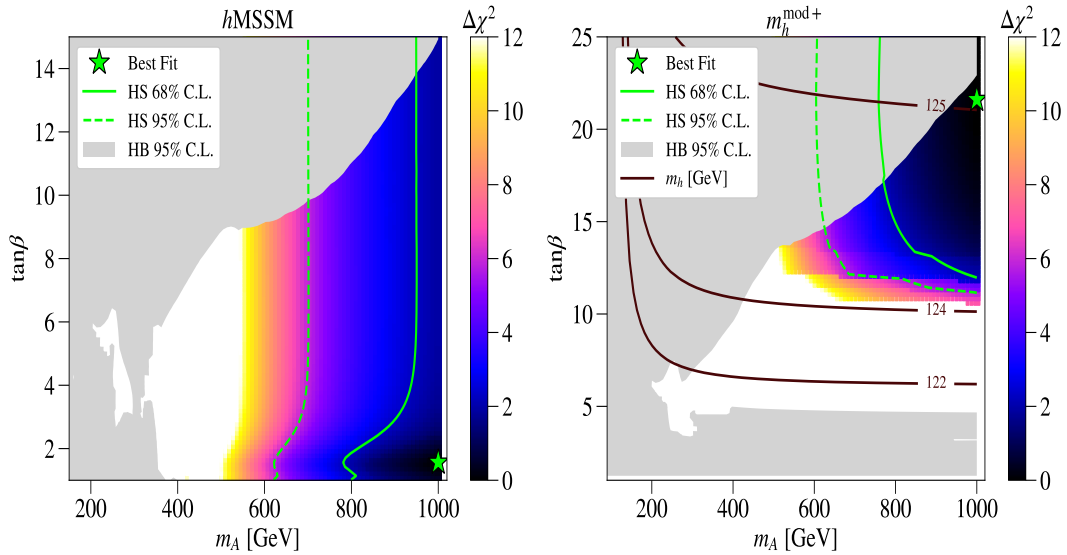


Figure 1: The allowed regions on the $(m_A, \tan\beta)$ plane in hMSSM (left) and $m_h^{\text{mod+}}$ (right). The cyan lines in the right plot are level curves for the SM-like Higgs mass. By definition, in the hMSSM, m_h is fixed at 125 GeV.

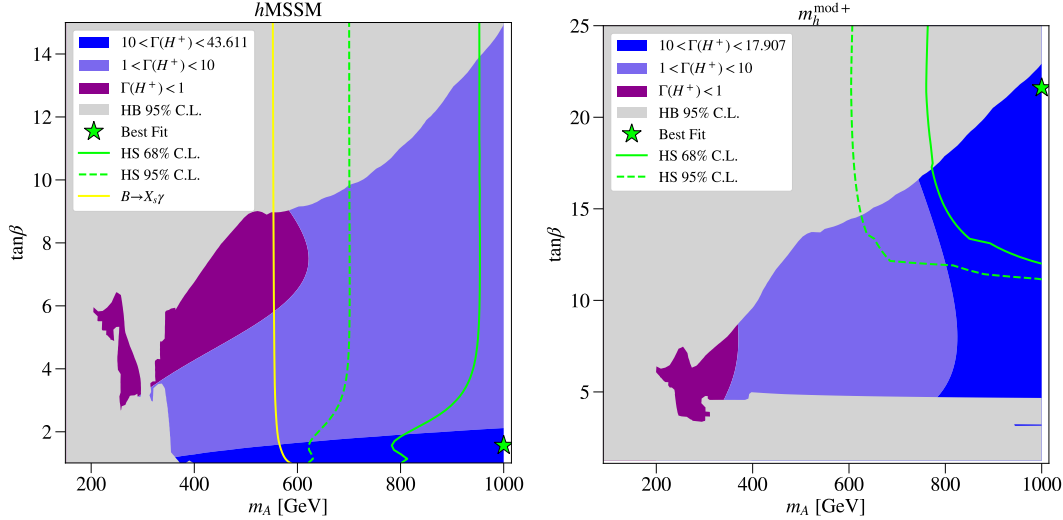


Figure 2: Total charged Higgs boson width (in GeV) mapped on the $(m_A, \tan \beta)$ plane in hMSSM (left) and $m_h^{\text{mod}+}$ (right). The units of Γ_{H^\pm} in the legends are intended in GeV.

In Fig. 1 the allowed regions on the $(m_A, \tan \beta)$ plane are depicted for various $\Delta\chi^2$, wherein the left and right panel are, respectively, for the hMSSM and $m_h^{\text{mod}+}$ scenarios. For the hMSSM and $\Delta\chi^2 \leq 12$, one can see that m_A should be heavier than about 400 GeV. In the case of $m_A \approx 400 - 600$ GeV, $\tan \beta$ should be in the range $[1, 9]$ while for m_A around 1 TeV $\tan \beta$ is in the range $[1, 15]$. The dash(solid) line represents the 95%(68%) CL obtained by the HiggsSignals fit and the best fit point is located at $m_A \approx 1$ TeV and $\tan \beta \approx 2$. For the $m_h^{\text{mod}+}$ scenario, the situation is quite different. In order to accommodate $m_h \approx 125$ GeV, one needs $\tan \beta > 10$. Similarly to the left panel, the dash(solid) line represents the 95%(68%) CL obtained by the HiggsSignals fit and the best fit point is located at $m_A \approx 1$ TeV and $\tan \beta \approx 20$. For this scenario and for $\Delta\chi^2 < 12$, all $\tan \beta \leq 10$ are excluded.

In Fig. 2 we present the total width of the charged Higgs boson, again, over the $(m_A, \tan \beta)$ plane, for both hMSSM (left) and $m_h^{\text{mod}+}$ (right). As one can see from the left panel, the total width for the hMSSM case is largest for $\tan \beta \leq 3$, which is when $\Gamma_{H^\pm} \approx 7 - 10$ GeV, while for $\tan \beta \geq 5$ the width drops to 1-3 GeV. This effect can be attributed to the fact that the total width is fully dominated by $H^+ \rightarrow t\bar{b}$, whenever this channel is open, in which the top effect is more pronounced for low $\tan \beta$. In this case, $H^+ \rightarrow \tau\nu$ is subleading and also the decay modes $H^+ \rightarrow \chi_i^+ \chi_j^0$ are suppressed. In the case of $m_h^{\text{mod}+}$, since small $\tan \beta$ is not allowed, the total charged Higgs boson width is generally smaller than in the hMSSM case, as a consequence of the fact that $H^+ \rightarrow t\bar{b}$ is therefore smaller in this scenario. The maximal total width is here obtained for $m_A \approx 1$ TeV and a large $\tan \beta \approx 20$. In the $m_h^{\text{mod}+}$ scenario, the decay $H^+ \rightarrow \chi_2^+ \chi_2^0$ could have a significant BR, reaching 30%. Hence, the H^\pm is always rather narrow, whichever its mass. In fact, owing to the degeneracy between m_A and m_{H^\pm} in the MSSM, as dictated by h data, a remarkable result is that in the minimal SUSY scenario a charged Higgs boson is essentially always heavier than the top quark.

In Fig. 3 we show the production cross section for single charged Higgs boson production in association with top quark (as appropriate for the $m_{H^\pm} > m_t$ case) times the BR of H^+ into a specific final state for both the hMSSM and $m_h^{\text{mod}+}$ scenarios. In fact, as we have seen previously, the total width of the charged Higgs state is rather small in both cases, in relation to the mass, so that one can use the Narrow Width Approximation (NWA) to estimate such a cross section (which we have done here). In the top-left(top-right) panel of Fig. 3, we show the size of the cross section of $\sigma(pp \rightarrow tH^\pm + \text{c.c.}) \times \text{BR}(H^\pm \rightarrow t\bar{b})$ ($\sigma(pp \rightarrow tH^- + \text{c.c.}) \times \text{BR}(H^\pm \rightarrow \tau\nu)$), given in pb.

For the hMSSM scenario, one can see that in the $t\bar{b}$ channel the largest cross section (more than 0.1

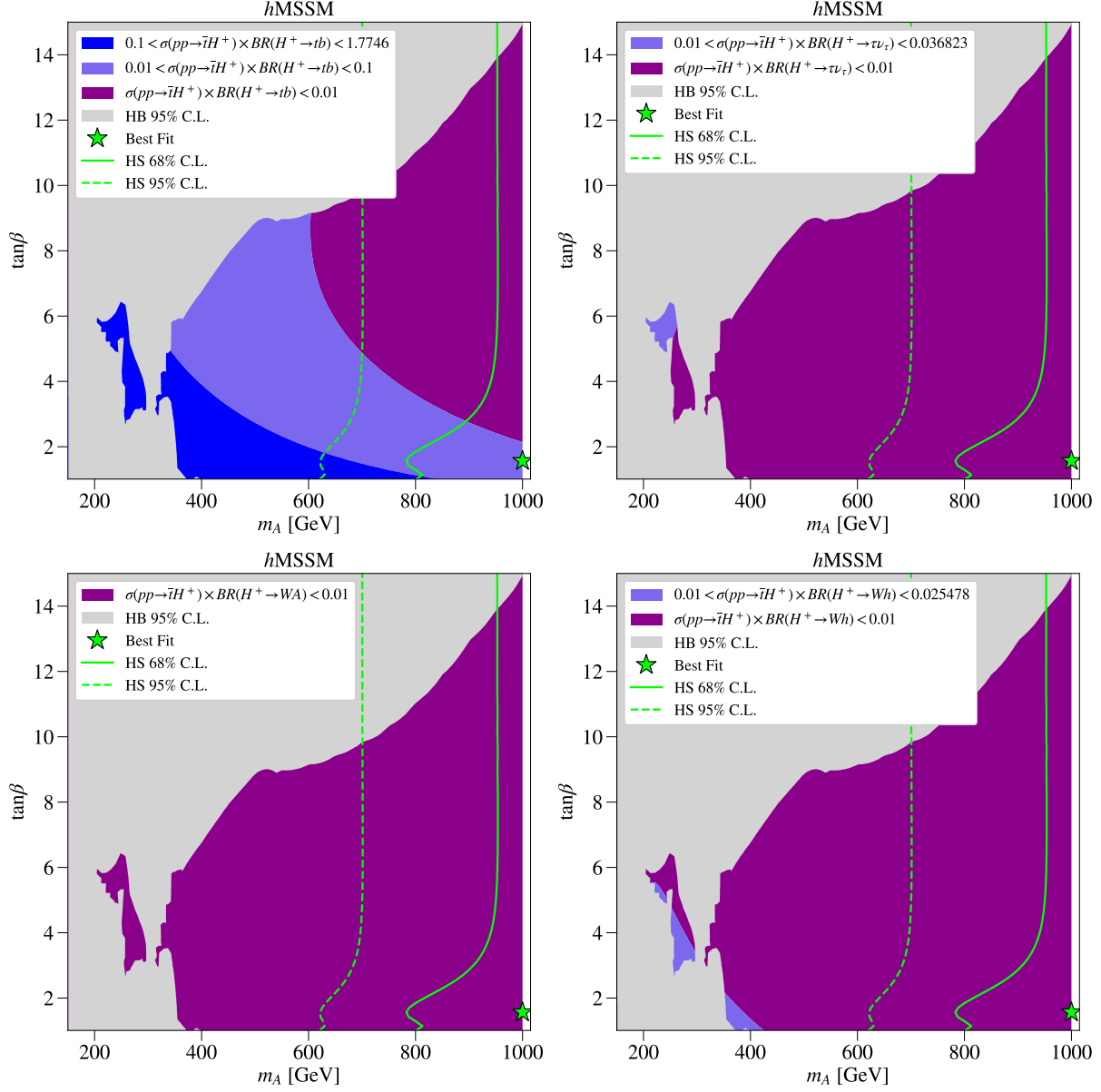


Figure 3: The $\sigma(pp \rightarrow tH^+ + \text{c.c.}) \times BR(H^\pm \rightarrow XY)$ rate (in pb) at $\sqrt{s}=14$ TeV in the hMSSM scenario, for $XY \equiv tb$ (top left), $XY \equiv \tau\nu$ (top right), $XY \equiv AW^\pm$ (bottom left) and $XY \equiv hW^\pm$ (bottom right). Notice that c.c. channels are included.

pb) is reached for small $\tan\beta < 3$. There is also a wide region with $m_{H^\pm} \in [400, 600]$ GeV and $\tan\beta < 10$ where the cross section is still rather important: between 10^{-3} and 0.1 pb. As for the $\tau\nu$ channel, the cross section is maximised when $\tan\beta$ is in the range [4, 9] and the largest cross section is seen around 10^{-3} pb. However, amongst the bosonic channels, $H^\pm \rightarrow W^\pm A$ is hopeless because $BR(H^\pm \rightarrow W^\pm A)$ is very suppressed while $H^\pm \rightarrow W^\pm h$ can have a rate that is close to 10^{-2} pb for small $\tan\beta \approx 1$. Note that, for completeness, we have also drawn the exclusion region due to $BR(\bar{B} \rightarrow X_s \gamma)$, even though we can always assume some kind of flavor violation that takes place in the MSSM and can bring the

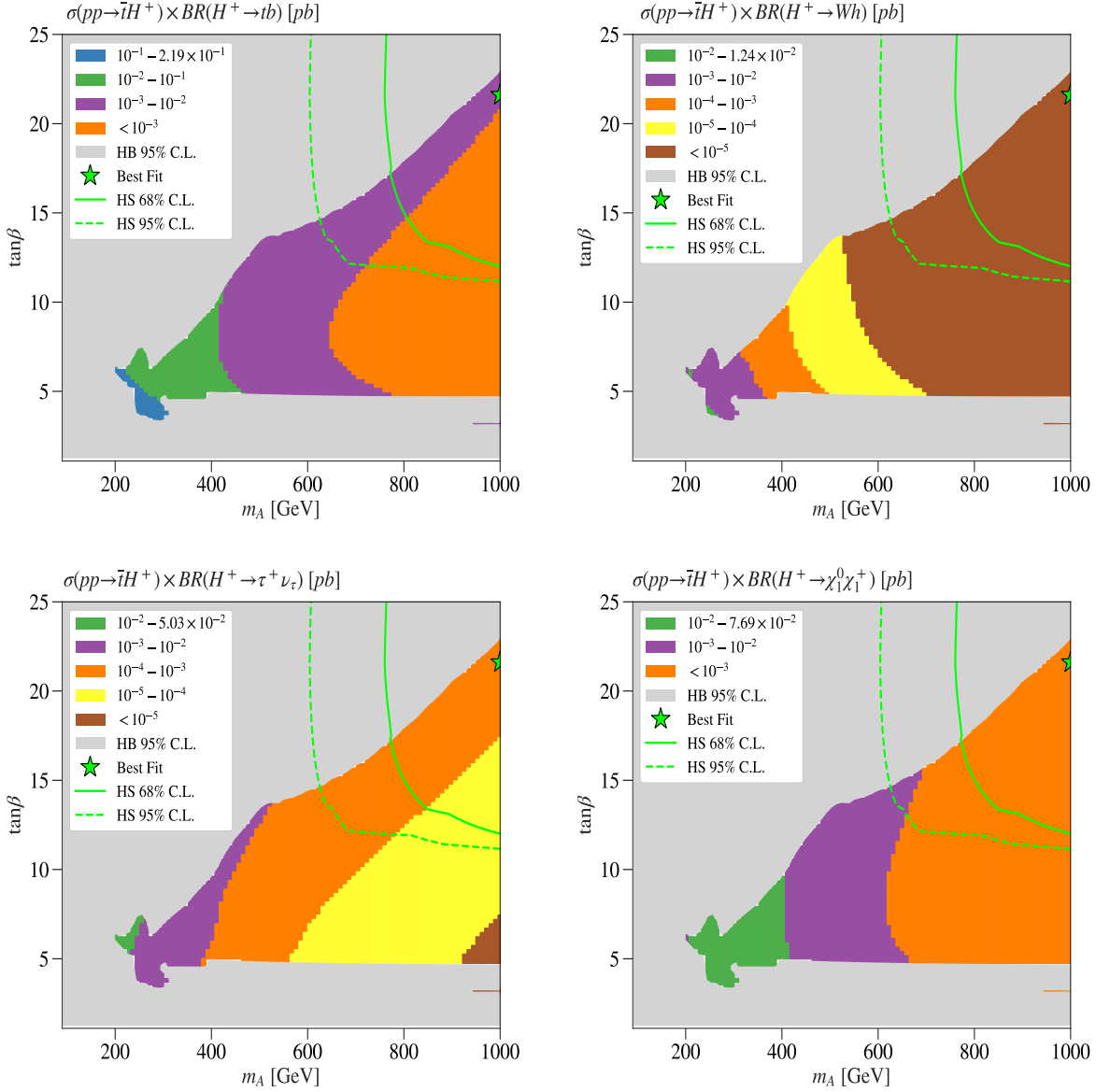


Figure 4: The $\sigma(pp \rightarrow tH^+ + \text{c.c.}) \times \text{BR}(H^\pm \rightarrow XY)$ rate (in pb) at $\sqrt{s}=14$ TeV in the $m_h^{\text{mod}+}$ scenario, for $XY \equiv tb$ (top left), $XY \equiv W^\pm h$ (top right), $XY \equiv \tau\nu$ (bottom left) and $XY \equiv \chi_1^0 \chi_1^+$ (bottom right). Notice that c.c. channels are included.

$\text{BR}(\bar{B} \rightarrow X_s \gamma)$ to a correct value. In terms of $\sigma(pp \rightarrow tH^+ + \text{c.c.}) \times \text{BR}(H^\pm \rightarrow XY)$ for the $m_h^{\text{mod}+}$ scenario, the situation is worse. The best channels are $H^+ \rightarrow t\bar{b}$ and $H^+ \rightarrow \chi_1^+ \chi_1^0$ with the maximum cross section in the allowed region being between 10^{-3} and 10^{-2} pb for charged Higgs boson masses in the range 400 to 600 GeV, as can be seen from Fig. 4.

We conclude this section by presenting in Tab. 2 two BPs, one each for the $m_h^{\text{mod}+}$ and hMSSM scenarios, to aid future analyses of Run-2 (and possibly Run-3) data from the LHC. Notice that these BPs do not correspond to the best fit points in these two MSSM configurations, as these would yield

Parameters	$m_h^{\text{mod}+}$	hMSSM
MSSM inputs		
$\tan \beta$	13.606	1.1414
M_{A^0} (GeV)	522.02	425.51
μ (GeV)	200	200
M_2 (GeV)	200	200
M_3 (GeV)	1500	1500
$A_t = A_b = A_\tau$ (GeV)	1514.7	2175.2
$M_{Q_{1,2}} = M_{U_{1,2}} = M_{D_{1,2}}$ (GeV)	1500	1500
$M_{Q_3} = M_{U_3} = M_{D_3}$ (GeV)	1000	1000
$M_{L_{1,2}} = M_{E_{1,2}}$ (GeV)	500	500
$M_{L_3} = M_{E_3}$ (GeV)	1000	1000
Masses in GeV		
M_{h^0}	124.5	125
M_{H^0}	522.04	451.09
M_{A^0}	522.02	425.51
M_{H^\pm}	528.22	433.04
$M_{\tilde{\chi}_1^+}$	145.93	119.88
$M_{\tilde{\chi}_2^+}$	267.64	280.26
$M_{\tilde{\chi}_1^0}$	87.218	71.894
$M_{\tilde{\chi}_2^0}$	150.45	138.44
$M_{\tilde{\chi}_4^0}$	267.56	285.23
$M_{\tilde{b}_1}$	998.5	1034.3
$M_{\tilde{b}_2}$	1003.6	1038.7
$M_{\tilde{\tau}_1}$	999.95	998.41
$M_{\tilde{\tau}_2}$	1002.1	1001.9
$M_{\tilde{t}_1}$	876.44	899.94
$M_{\tilde{t}_2}$	1134.8	1173.7
Total decay width in GeV		
Γ_{H^\pm}	4.6041	13.742
Charged Higgs BRs in %		
$\text{BR}(H^+ \rightarrow t\bar{b})$	24.04	98.9
$\text{BR}(H^+ \rightarrow \tilde{\chi}_1^+ \tilde{\chi}_3^0)$	11.7	–
$\text{BR}(H^+ \rightarrow \tilde{\chi}_1^+ \tilde{\chi}_4^0)$	15.12	–
$\text{BR}(H^+ \rightarrow \tilde{\chi}_1^0 \tilde{\chi}_1^+)$	12.13	–
$\text{BR}(H^+ \rightarrow \tilde{\chi}_2^0 \tilde{\chi}_2^+)$	23.54	–
$\text{BR}(H^+ \rightarrow \tilde{\chi}_3^0 \tilde{\chi}_2^+)$	6.49	–
$\text{BR}(H^+ \rightarrow \tau^+ \nu_\tau)$	4.25	8.51×10^{-3}
Cross section in pb		
$\sigma(pp \rightarrow tH^+ + \text{c.c.})$	0.0246	0.9583

Table 2: BPs for the $m_h^{\text{mod}+}$ and hMSSM scenarios.

too small cross sections⁹, owing to the very large charged Higgs mass involved (of order 1 TeV). Yet, the BPs presented correspond to rather large values of m_{H^\pm} , as dictated by the compatibility tests of the $m_h^{\text{mod}+}$ and hMSSM scenarios with current datasets, still giving production and decay rates (in one or more channels) potentially testable in the near future.

⁹Probably accessible only at the High-Luminosity LHC [108].

m_h (GeV)	m_H (GeV)	m_A (GeV)	m_{H^\pm} (GeV)	α	β	m_{12}^2 (GeV ²)
125	$[m_{H^\pm}; 1000]$	$[90; m_{H^\pm}]$	$[90; 1000]$	$[\pi/5; \pi/2]$	$[-\pi/2; \pi/2]$	$m_A^2 \tan\beta/(1 + \tan^2\beta)$

Table 3: Allowed range of variation for the free parameters.

4.5 2HDM results

4.5.1 Parameters regions

We now move on to discuss the 2HDM. In this scenario, we consider h as being again the 125 GeV SM-Higgs like and vary the other six parameters as indicated in Tab. 3. When performing the scan over the 2HDM parameter space, other than taking into account the usual LHC, Tevatron and LEP bounds (as implemented in HiggsBounds and HiggsSignals) as well as the theoretical ones (as implemented in 2HDMC), we also have to consider flavor observables. In fact, unlike the MSSM, where potentially significant contributions to (especially) B -physics due to the additional Higgs states entering the 2HDM beyond the SM-like one can be cancelled by the corresponding sparticle effects (and besides, are generally small because of the rather heavy H, A and H^\pm masses), the 2HDM has to be tested against a variety of data. The B -physics observables that we have considered to that effect are listed in Tab. 4. We have computed the 2HDM predictions for these in all 2HDM Types using our own implementation, which output in fact agrees with the one from SuperIso [109] (when run in 2HDM mode).

Based on such constrained scans, we first illustrate in Fig. 5, on the (α, β) plane, the best fit points for the four 2HDM Types. Herein, are also shown the compatibility regions with the observed Higgs signal at the 1σ (green) and 2σ level (yellow). The details of the best fit points herein (red stars) are given in Tab. 5 together with the values of the following observables: the total charged Higgs width Γ_{H^\pm} , $\sigma(pp \rightarrow tH^- + c.c.)$, $\text{BR}(H^\pm \rightarrow \tau\nu)$, $\text{BR}(H^\pm \rightarrow AW^\pm)$, $\text{BR}(H^\pm \rightarrow tb)$ and $\text{BR}(H^\pm \rightarrow hW^\pm)$. Note that in the 2HDM Type-II and -Y, the best fit point is located at a charged Higgs mass around 600 GeV because of the $\bar{B} \rightarrow X_s\gamma$ constraints while in the 2HDM Type-I and -X one can fit data with a rather light charged Higgs state.

Observable	Experimental result	SM contribution	Combined at 1σ
$\text{BR}(B \rightarrow \tau\nu)$	$(1.14 \pm 0.22) \times 10^{-4}$ [105]	$(0.78 \pm 0.07) \times 10^{-4}$	0.23×10^{-4}
$\text{BR}(B_s^0 \rightarrow \mu^+\mu^-)$	$(2.8 \pm 0.7) \times 10^{-9}$ [106]	$(3.66 \pm 0.28) \times 10^{-9}$	0.75×10^{-9}
$\text{BR}(B_d^0 \rightarrow \mu^+\mu^-)$	$(3.9 \pm 1.5) \times 10^{-10}$ [106]	$(1.08 \pm 0.13) \times 10^{-10}$	1.50×10^{-10}
$\text{BR}(\bar{B} \rightarrow X_s\gamma)_{E_\gamma > 1.6 \text{ GeV}}$	$(3.43 \pm 0.22) \times 10^{-4}$ [105]	$(3.36 \pm 0.24) \times 10^{-4}$	0.32×10^{-4}
ΔM_s	$(17.757 \pm 0.021) \text{ ps}^{-1}$ [107, 105]	$(18.257 \pm 1.505) \text{ ps}^{-1}$	1.5 ps^{-1}
ΔM_d	$(0.510 \pm 0.003) \text{ ps}^{-1}$ [107, 105]	$(0.548 \pm 0.075) \text{ ps}^{-1}$	0.075 ps^{-1}

Table 4: Experimental results of flavor observables combined by the PDG and/or HFAG collaborations in Refs. [105, 107]. As for $\text{BR}(B_q^0 \rightarrow \mu^+\mu^-)$, the combined results from the LHCb and CMS collaborations are shown as in Ref. [106].

In Fig. 6(Fig. 7)[Fig. 8]{Fig. 9}, we show (in gray) over the $(m_{H^\pm}, \tan\beta)$ plane the 95% CL exclusion region from the non-observation of the additional Higgs states for 2HDM Type-I(-II)[-X]{-Y}. In all these plots, we also draw (as a solid yellow line) the 95% CL exclusion from $\text{BR}(\bar{B} \rightarrow X_s\gamma)$ together with a solid green line representing the 1σ compatibility with the Higgs signals observed at the LHC. As a green star, we also give the best fit point to these data over the available parameter space for all Types (these are the same as the red stars in the previous figure). It is clear from these plots that, in the 2HDM-I and -X, one can still have relatively light charged Higgs states (of the order 100 to 200 GeV in mass) that are consistent with all aforementioned data, crucially including B -physics observables. In the case of the 2HDM Type-II and -Y, the $\text{BR}(\bar{B} \rightarrow X_s\gamma)$ constraint pushes the charged Higgs boson mass to be higher than 580 GeV. (Note that, in the 2HDM Type-II, it is clear that, like for the MSSM case, large $\tan\beta$ is

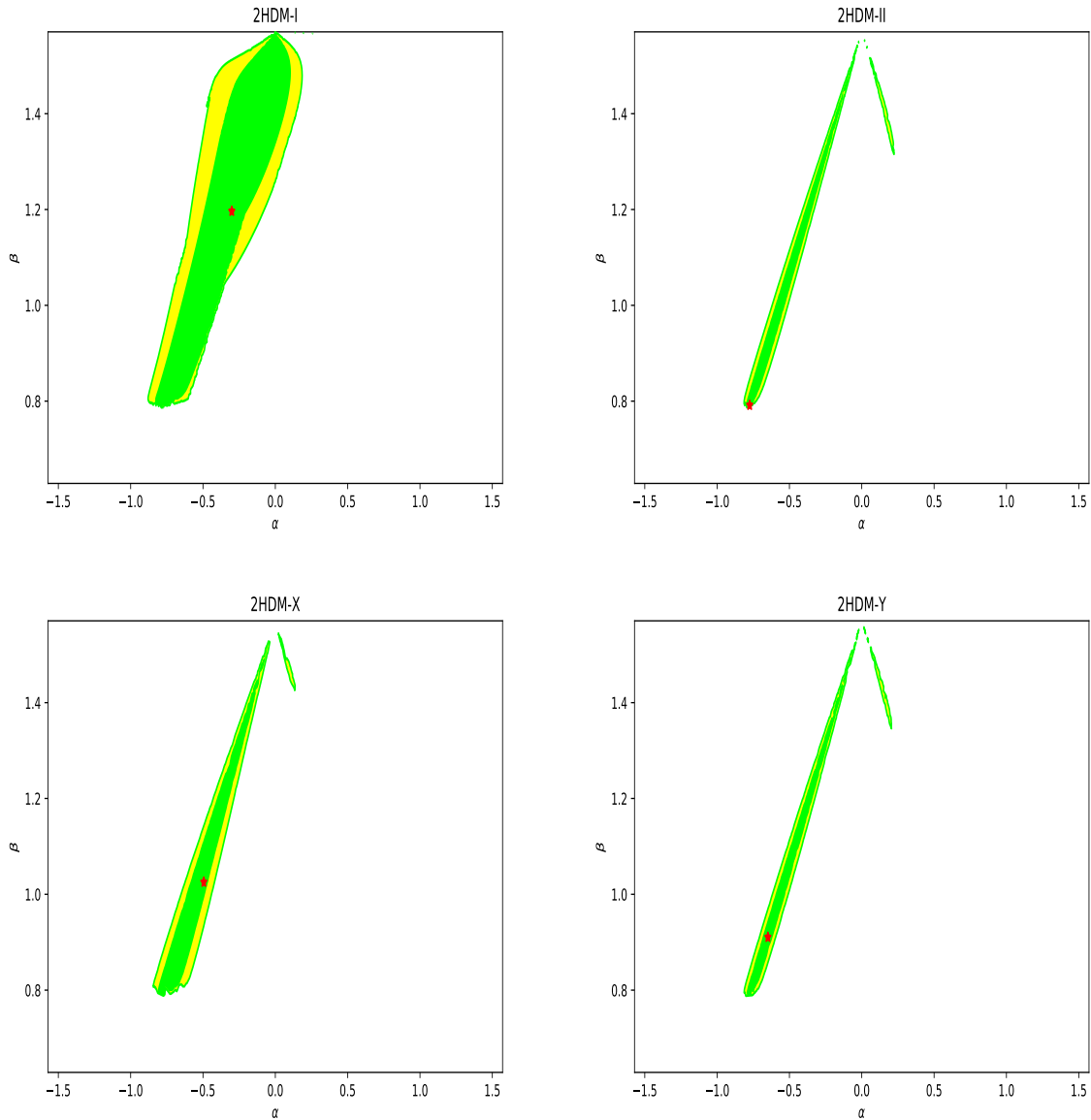


Figure 5: Direct constraints from null heavy Higgs searches at the LHC on the parameter space of the 2HDM Type-I (top left), Type-II (top right), Type-X (bottom left) and Type-Y (bottom right) mapped on the (α, β) plane. The colors indicate compatibility with the observed Higgs signal at 1σ (green), 2σ (yellow) around the best fit points (red stars).

excluded mainly from $H, A \rightarrow \tau^+\tau^-$ as well as from $H^\pm \rightarrow \tau\nu$ searches at LHC). However, for 2HDM Type-X, one can see that light charged Higgs states, with $m_{H^\pm} \leq 170$ GeV, are excluded for all $\tan\beta$'s and this is due to charged Higgs searches failing to detect $H^\pm \rightarrow \tau\nu$.

We now discuss the size of the charged Higgs production cross section times its BRs in decay channels such as $H^+ \rightarrow t\bar{b}, \tau\nu, AW^\pm$ and hW^\pm . In Fig. 6(top-left panel) we illustrate the values of $\sigma(pp \rightarrow tH^- + \text{c.c.}) \times \text{BR}(H^\pm \rightarrow tb)$ (in pb) where we can see that it is possible to have a production times decay rate in the range 0.01 to 0.2 pb for $1 \leq \tan\beta \leq 6$ and $180 \text{ GeV} < m_{H^\pm} < 300 \text{ GeV}$. This could

Parameters	Type-I	Type-II	Type-X	Type-Y
(α, β)	(-0.30107, 1.19645)	(-0.77474, 0.791554)	(-0.49444, 1.02543)	(-0.64861, 0.91044)
$(m_{H^\pm}, \Gamma_{H^\pm})$ (GeV)	(178, 1.4×10^{-2})	(592, 25.2)	(493, 7.63)	(631, 16.8)
(m_A, m_H) (GeV)	(97.71, 212)	(512, 694)	(412, 509)	(550, 652)
$\text{BR}(H^\pm \rightarrow \tau\nu)$	0.4%	–	0.03%	–
$\text{BR}(H^\pm \rightarrow AW^\pm)$	55.2%	0.05%	0.18%	0.08%
$\text{BR}(H^\pm \rightarrow hW^\pm)$	0.01%	0.04%	0.9%	0.06%
$\text{BR}(H^\pm \rightarrow tb)$	44.1%	99.7%	98.6%	99.6%
$\sigma(pp \rightarrow tH^- + \text{c.c.})$ (fb)	1570	434	308	214

Table 5: The best fit points in the 2HDM Type-I, -II, -X and -Y. The decay width Γ_{H^\pm} , cross sections $\sigma(pp \rightarrow tH^- + \text{c.c.})$ as well as relevant decay BRs for the charged Higgs state are listed, for which values smaller than 10^{-4} are neglected. We have fixed $m_h = 125$ GeV and $m_{12}^2 = m_A^2 \sin\beta \cos\beta$.

lead to more than thousands raw $t\bar{b}$ signal events for 100 fb^{-1} luminosity. In the case of $H^\pm \rightarrow \tau\nu$ and $H^\pm \rightarrow hW^\pm$, which are suppressed, respectively, by $1/\tan\beta$ and $\cos(\beta - \alpha) \approx 0$, the rate is much smaller than for the tb mode. In contrast, since the coupling $H^\pm W^\mp A$ is a gauge coupling without any suppression factor, when $H^\pm \rightarrow AW^\pm$ is open, it may dominate over the $H^\pm \rightarrow tb$ channel. One can see from Fig. 6(bottom-left panel) that, for $100 \text{ GeV} < m_{H^\pm} < 220 \text{ GeV}$ and for all $1 \leq \tan\beta \leq 14$, the corresponding rate for $\sigma(pp \rightarrow tH^- + \text{c.c.}) \times \text{BR}(H^\pm \rightarrow AW^\pm) \geq 0.01 \text{ pb}$. This could lead to an interesting final state bW^+W^-A where one W^\pm could be decay leptonically. The decay $H^\pm \rightarrow hW^\pm$ is essentially inaccessible, see Fig. 6(bottom-right panel).

In the case of 2HDM Type-II and -Y, as one can see from Fig. 7 and Fig. 9, respectively, that there is a wide region over the $(m_{H^\pm}, \tan\beta)$ plane where the rate for $\sigma(pp \rightarrow tH^- + \text{c.c.}) \times \text{BR}(H^\pm \rightarrow tb)$ is rather sizable for both moderate ($m_{H^\pm} \leq 300 \text{ GeV}$) and heavy (otherwise) charged Higgs masses (top-left panel). However, if one takes into account the $\bar{B} \rightarrow X_s \gamma$ constraint, then m_{H^\pm} is required to be much heavier than 580 GeV (as already discussed), which makes the rate $\sigma(pp \rightarrow tH^- + \text{c.c.}) \times \text{BR}(H^\pm \rightarrow tb) \geq 0.1 \text{ pb}$ only for $\tan\beta < 1.5$. All the other channels (in the three remaining panels) have smaller production times decay rates.

The 2HDM Type-X is depicted in Fig. 8, wherein the usual production times BR rates are shown. The top-right panel is again for the $H^+ \rightarrow t\bar{b}$ channel, which exhibits a potentially interesting cross section ($\geq 1 \text{ fb}$) in the $H^+ \rightarrow t\bar{b}$ channel for both a light charged Higgs mass (around 200 GeV) and a heavy one (around 420 GeV). In the case of the $\tau\nu$ channel (top-right panel), one can get sizable rates for $\sigma(pp \rightarrow tH^- + \text{c.c.}) \times \text{BR}(H^\pm \rightarrow \tau\nu)$ for a charged Higgs mass around 200 GeV and $\tan\beta \geq 2$.

5 Conclusions

We have studied charged Higgs boson phenomenology in both the MSSM and 2HDM, the purpose being to define BPs amenable to phenomenological investigation already with the full Run-1 and 2 dataset and certainly accessible with the Run-3 one of the LHC. They have been singled out following the enforcement of the latest theoretical and experimental constraints, so as to be entirely up-to-date. Furthermore, they

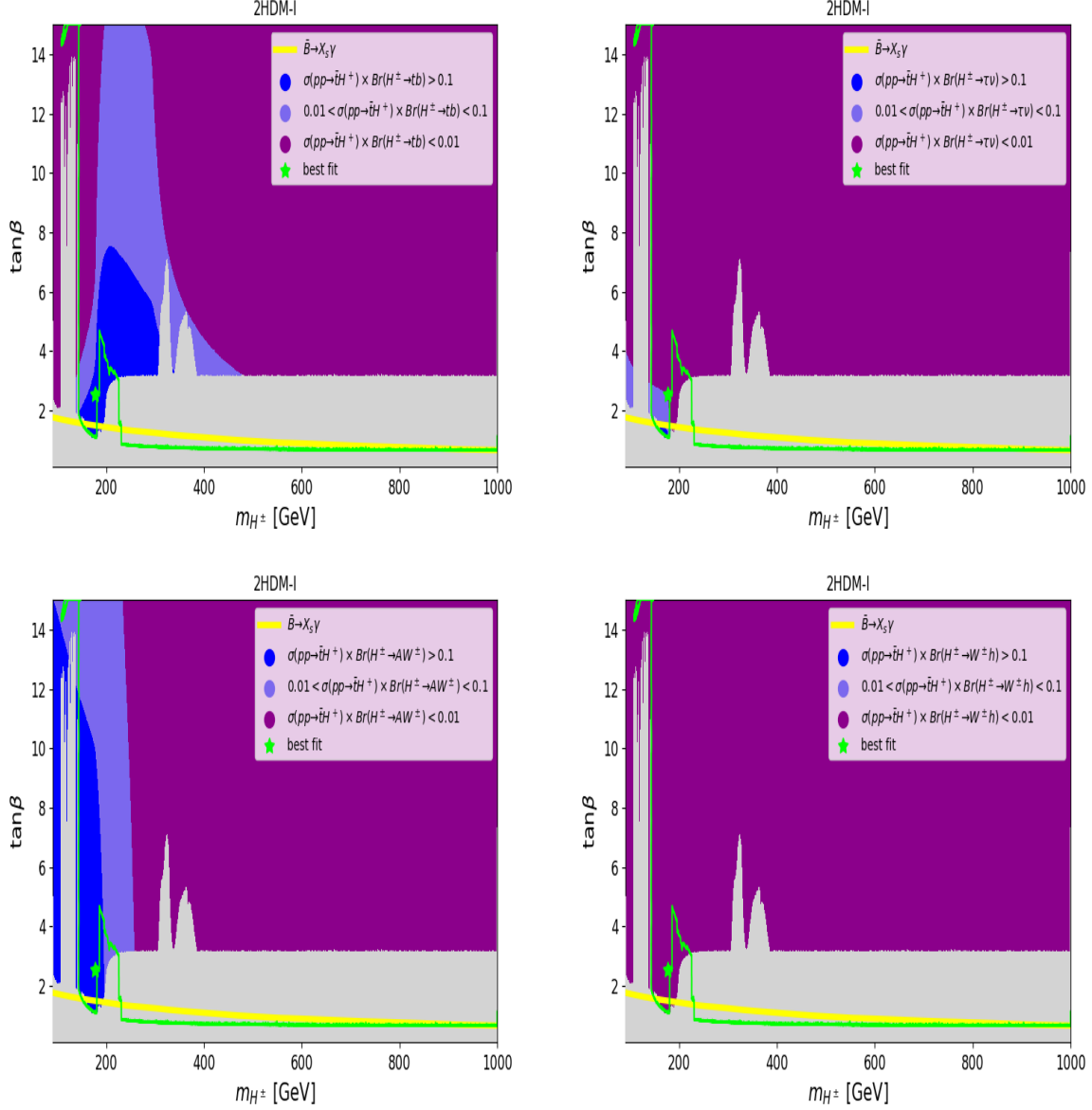


Figure 6: The $\sigma(pp \rightarrow tH^- + \text{c.c.}) \times \text{BR}(H^\pm \rightarrow XY)$ rate (in pb) at $\sqrt{s}=14$ TeV in the 2HDM Type-I, for $XY \equiv tb$ (top left), $XY \equiv \tau\nu$ (top right), $XY \equiv AW^\pm$ (bottom left) and $XY \equiv hW^\pm$ (bottom right). Exclusion bounds at 95% CL from the non-observation of the additional Higgs states are overlaid in gray. The green contour indicates compatibility with the observed Higgs signal at 1σ and the best fit (benchmark) points are marked by red stars. The solid yellow line contours are the boundary of 95% CL exclusion from $\bar{B} \rightarrow X_s\gamma$ measurements. The maximum of the cross section $\sigma(pp \rightarrow tH^- + \text{c.c.}) \times \text{BR}(H^\pm \rightarrow XY)$ is 3.1 pb and 1.83 pb for $XY \equiv AW^\pm, tb$, respectively.

have been defined with the intent of increasing sensitivity of dedicated (model-dependent) H^\pm searches to some of the most probable parameter space configurations of either scenario. With this in mind, we have listed in two tables their input and output values, the former in terms of the fundamental parameters of the model concerned and the latter in terms of key observables (like, e.g., physical masses and couplings,

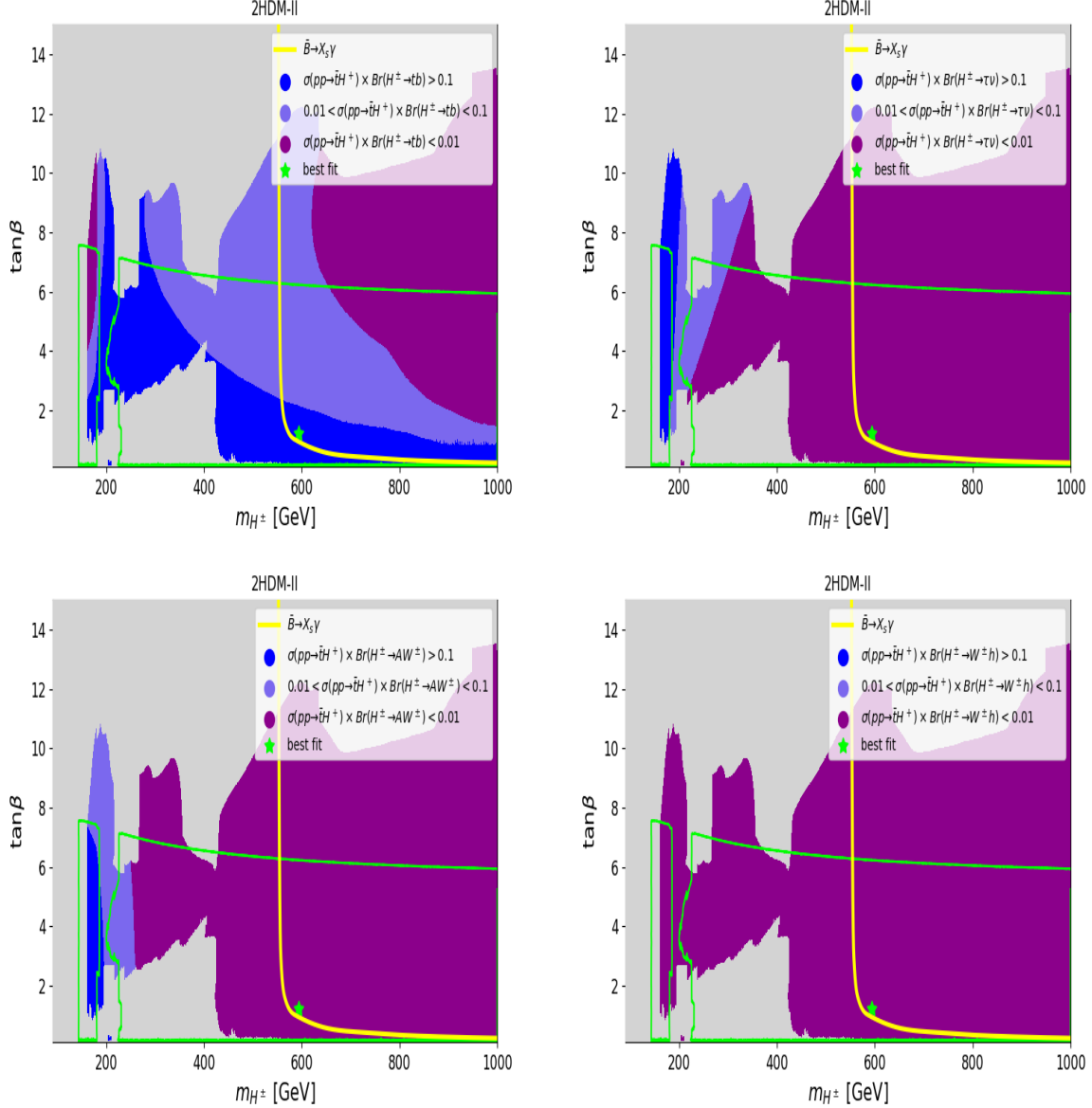


Figure 7: The $\sigma(pp \rightarrow tH^\pm + \text{c.c.}) \times \text{BR}(H^\pm \rightarrow XY)$ rate (in pb) at $\sqrt{s}=14$ TeV in the 2HDM Type-II, for $XY \equiv tb$ (top left), $XY \equiv \tau\nu$ (top right), $XY \equiv AW^\pm$ (bottom left) and $XY \equiv hW^\pm$ (bottom right). The maximum of the cross section $\sigma(pp \rightarrow tH^\pm + \text{c.c.}) \times \text{BR}(H^\pm \rightarrow XY)$ is 2.3 pb and 1.38 pb for $XY \equiv AW^\pm, tb$, respectively. The color coding is the same as in Fig. 6.

production cross sections and decay BRs). We have also specified which numerical tools we have used to produce all such an information, including their settings.

For the MSSM we have concentrated on two popular scenarios, i.e., the hMSSM and $m_h^{\text{mod}+}$ ones. It was found that the hMSSM case still possesses a rather large available parameter space, here mapped over the $(m_A, \tan\beta)$ plane, while the $m_h^{\text{mod}+}$ one is instead much more constrained. In terms of the largest production and decay rates, in the hMSSM scenario one finds that the most copious channels, assuming $pp \rightarrow tH^- + \text{c.c.}$ production, are via the decay $H^+ \rightarrow t\bar{b}$ followed by $H^+ \rightarrow \tau\nu$ whereas for

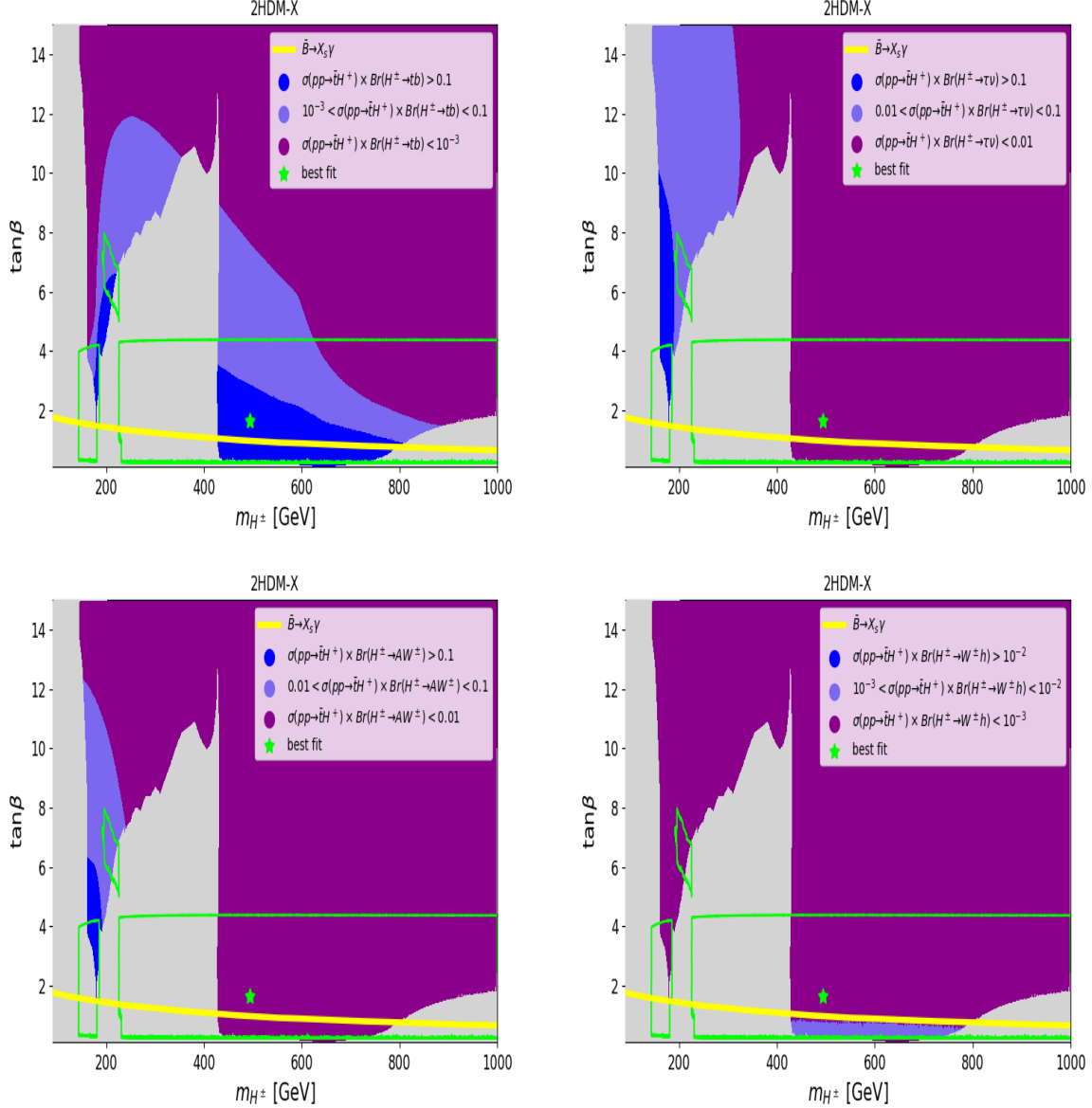


Figure 8: The $\sigma(pp \rightarrow tH^- + \text{c.c.}) \times \text{BR}(H^\pm \rightarrow XY)$ rate (in pb) at $\sqrt{s}=14$ TeV in the 2HDM Type-X, for $XY \equiv tb$ (top left), $XY \equiv \tau\nu$ (top right), $XY \equiv AW^\pm$ (bottom left) and $XY \equiv hW^\pm$ (bottom right). The maximum of the cross section $\sigma(pp \rightarrow tH^- + \text{c.c.}) \times \text{BR}(H^\pm \rightarrow XY)$ is 2.3 pb and 1.23 pb for $XY \equiv AW^\pm, tb$, respectively. The color coding is the same as in Fig. 6.

the $m_h^{\text{mod}+}$ scenario the decay modes $H^+ \rightarrow t\bar{b}$ and $H^+ \rightarrow \chi_1^+ \chi_0$ offer the largest rates. In both cases, only $m_{H^\pm} > m_t$ values are truly admissible by current data.

Within the 2HDM, we have looked at the four standard Yukawa setups, known as Type-I, -II, -X and -Y. Because of $\bar{B} \rightarrow X_s \gamma$ constraints, the profile of a charged Higgs in the 2HDM Type-II and -Y is a rather heavy one, with a mass required to be more than 580 GeV. While this puts an obvious limit to LHC sensitivity owing to a large phase space suppression in production, we have emphasised that $H^\pm \rightarrow b\bar{b}W^\pm$ channels should be searched for, with intermediate contributions from the AW^\pm and tb

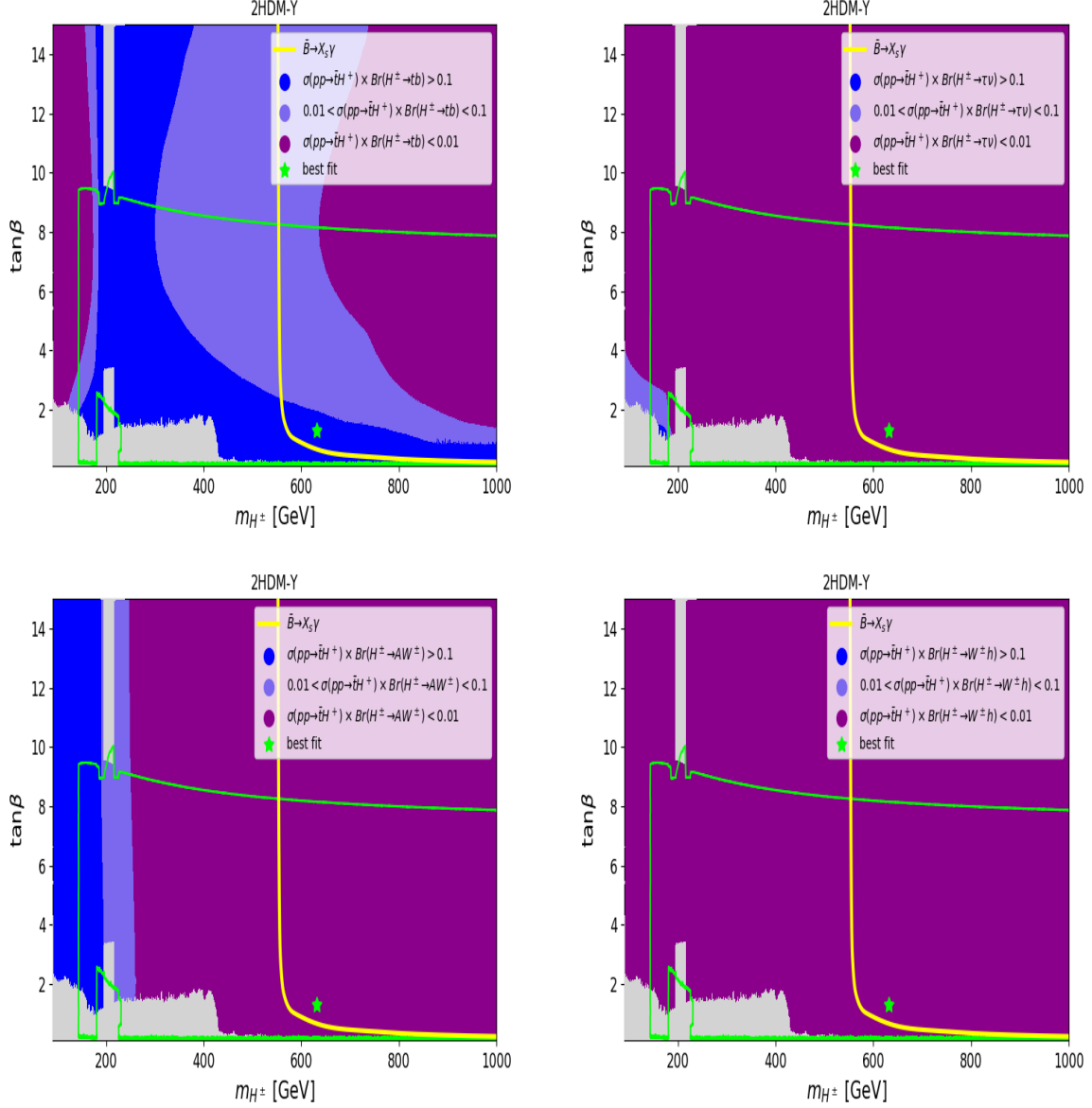


Figure 9: The $\sigma(pp \rightarrow tH^- + \text{c.c.}) \times \text{BR}(H^\pm \rightarrow XY)$ rate (in pb) at $\sqrt{s}=14$ TeV in the 2HDM Type-Y, for $XY \equiv tb$ (top left), $XY \equiv \tau\nu$ (top right), $XY \equiv AW^\pm$ (bottom left) and $XY \equiv hW^\pm$ (bottom right). The maximum of the cross section $\sigma(pp \rightarrow tH^- + \text{c.c.}) \times \text{BR}(H^\pm \rightarrow XY)$ is 3.54 pb and 1.85 pb for $XY \equiv AW^\pm, tb$, respectively. The color coding is the same as in Fig. 6.

modes (including their interference [110]), alongside $H^\pm \rightarrow \tau\nu$. In the case of the 2HDM Type-I and -X, a much lighter charged Higgs state is still allowed by data, in fact, even with a mass below that of the top quark. While the configuration $m_{H^\pm} < m_t$ is best probed by using $t\bar{t}$ production and decays into $\tau\nu$, the complementary mass region, i.e., $m_{H^\pm} > m_t$ (wherein $pp \rightarrow tH^- + \text{c.c.}$ is the production mode), may well be accessible via a combination of $H^+ \rightarrow t\bar{b}$ and $H^\pm \rightarrow AW^\pm$ (in Type-I) plus $H^\pm \rightarrow \tau\nu$ (in Type-X).

Acknowledgments

AA, RB and SM are supported by the grant H2020-MSCA-RISE-2014 no. 645722 (NonMinimalHiggs). This work is also supported by the Moroccan Ministry of Higher Education and Scientific Research MESRSFC and CNRST: Project PPR/2015/6. SM is supported in part through the NExT Institute and the STFC CG ST/L000296/1.

References

- [1] G. Aad *et al.* [ATLAS Collaboration], Phys. Lett. B **716**, 1 (2012) [arXiv:1207.7214 [hep-ex]].
- [2] G. Aad *et al.* [ATLAS Collaboration], Phys. Lett. B **726**, 88 (2013) [Erratum: Phys. Lett. B **734** (2014) 406] [arXiv:1307.1427 [hep-ex]].
- [3] S. Chatrchyan *et al.* [CMS Collaboration], Phys. Lett. B **716**, 30 (2012) [arXiv:1207.7235 [hep-ex]].
- [4] S. Chatrchyan *et al.* [CMS Collaboration], JHEP **1306**, 081 (2013) [arXiv:1303.4571 [hep-ex]].
- [5] S. P. Martin, Adv. Ser. Direct. High Energy Phys. **21**, 1 (2010) [Adv. Ser. Direct. High Energy Phys. **18**, 1 (1998)] [hep-ph/9709356].
- [6] The ATLAS collaboration [ATLAS Collaboration], ATLAS-CONF-2014-009.
- [7] CMS Collaboration [CMS Collaboration], CMS-PAS-HIG-14-009.
- [8] J. F. Gunion, H. E. Haber, G. L. Kane and S. Dawson, Front. Phys. **80**, 1 (2000).
- [9] M. Carena and H. E. Haber, Prog. Part. Nucl. Phys. **50**, 63 (2003) [hep-ph/0208209].
- [10] A. Djouadi, Phys. Rept. **459**, 1 (2008) [hep-ph/0503173].
- [11] M. Carena, S. Heinemeyer, C. E. M. Wagner and G. Weiglein, Eur. Phys. J. C **45**, 797 (2006) [hep-ph/0511023].
- [12] M. Carena, S. Heinemeyer, O. Stl, C. E. M. Wagner and G. Weiglein, Eur. Phys. J. C **73** no.9, 2552 (2013) [arXiv:1302.7033 [hep-ph]].
- [13] M. Carena, S. Heinemeyer, C. E. M. Wagner and G. Weiglein, Eur. Phys. J. C **26**, 601 (2003) [hep-ph/0202167].
- [14] A. Djouadi, L. Maiani, G. Moreau, A. Polosa, J. Quevillon and V. Riquer, Eur. Phys. J. C **73**, 2650 (2013) [arXiv:1307.5205 [hep-ph]].
- [15] E. Bagnaschi *et al.*, LHCHSWG-2015-002.
- [16] V. D. Barger, R. J. N. Phillips and D. P. Roy, Phys. Lett. B **324**, 236 (1994) [hep-ph/9311372]; J. F. Gunion, H. E. Haber, F. E. Paige, W. K. Tung and S. S. D. Willenbrock, Nucl. Phys. B **294**, 621 (1987); J. L. Diaz-Cruz and O. A. Sampayo, Phys. Rev. D **50**, 6820 (1994).
- [17] A. G. Akeroyd *et al.*, Eur. Phys. J. C **77** no.5, 276 (2017) [arXiv:1607.01320 [hep-ph]].
- [18] M. Guchait and S. Moretti, JHEP **0201**, 001 (2002) [hep-ph/0110020].
- [19] G. Aad *et al.* [ATLAS Collaboration], JHEP **1503**, 088 (2015) [arXiv:1412.6663 [hep-ex]].
- [20] V. Khachatryan *et al.* [CMS Collaboration], JHEP **1511**, 018 (2015) [arXiv:1508.07774 [hep-ex]].
- [21] G. Aad *et al.* [ATLAS Collaboration], Eur. Phys. J. C **73** no.6, 2465 (2013) [arXiv:1302.3694 [hep-ex]].

- [22] V. Khachatryan *et al.* [CMS Collaboration], JHEP **1512**, 178 (2015) [arXiv:1510.04252 [hep-ex]].
- [23] CMS Collaboration [CMS Collaboration], CMS-PAS-HIG-16-030.
- [24] M. Aaboud *et al.* [ATLAS Collaboration], Phys. Lett. B **759**, 555 (2016) [arXiv:1603.09203 [hep-ex]].
- [25] CMS Collaboration [CMS Collaboration], CMS-PAS-HIG-16-031.
- [26] The ATLAS collaboration [ATLAS Collaboration], ATLAS-CONF-2016-089.
- [27] A. Arhrib, R. Benbrik and S. Moretti, Eur. Phys. J. C **77**, no. 9, 621 (2017) [arXiv:1607.02402 [hep-ph]].
- [28] S. Heinemeyer, W. Hollik and G. Weiglein, Eur. Phys. J. C **9**, 343 (1999) [hep-ph/9812472].
- [29] S. Heinemeyer, W. Hollik and G. Weiglein, Phys. Rev. D **58**, 091701 (1998) [hep-ph/9803277].
- [30] S. Heinemeyer, W. Hollik and G. Weiglein, Phys. Lett. B **440**, 296 (1998) [hep-ph/9807423].
- [31] S. Heinemeyer, W. Hollik and G. Weiglein, Comput. Phys. Commun. **124**, 76 (2000) [hep-ph/9812320].
- [32] T. Hahn, S. Heinemeyer, W. Hollik, H. Rzehak and G. Weiglein, Comput. Phys. Commun. **180**, 1426 (2009).
- [33] R. V. Harlander, S. Liebler and H. Mantler, Comput. Phys. Commun. **184**, 1605 (2013) [arXiv:1212.3249 [hep-ph]].
- [34] R. V. Harlander, S. Liebler and H. Mantler, Comput. Phys. Commun. **212**, 239 (2017) [arXiv:1605.03190 [hep-ph]].
- [35] [ATLAS Collaboration], ATLAS-CONF-2013-007.
- [36] G. Aad *et al.* [ATLAS Collaboration], JHEP **1310**, 130 (2013) [Erratum: JHEP **1401**, 109 (2014)] [arXiv:1308.1841 [hep-ex]].
- [37] S. Chatrchyan *et al.* [CMS Collaboration], Eur. Phys. J. C **73**, no. 9, 2568 (2013) [arXiv:1303.2985 [hep-ex]].
- [38] S. Chatrchyan *et al.* [CMS Collaboration], JHEP **1401**, 163 (2014) [Erratum: JHEP **1501**, 014 (2015)] [arXiv:1311.6736, arXiv:1311.6736 [hep-ex]].
- [39] S. Chatrchyan *et al.* [CMS Collaboration], JHEP **1406**, 055 (2014) [arXiv:1402.4770 [hep-ex]].
- [40] J. F. Gunion and H. E. Haber, Phys. Rev. D **67**, 075019 (2003) [hep-ph/0207010].
- [41] G. C. Branco, L. Lavoura and J. P. Silva, Int. Ser. Monogr. Phys. **103**, 1 (1999).
- [42] M. Gomez-Bock and R. Noriega-Papaqui, J. Phys. G **32**, 761 (2006) [hep-ph/0509353].
- [43] A. Arhrib, R. Benbrik, C. H. Chen, J. K. Parry, L. Rahili, S. Semlali and Q. S. Yan, arXiv:1710.05898 [hep-ph].
- [44] P. M. Ferreira, J. F. Gunion, H. E. Haber and R. Santos, Phys. Rev. D **89**, no. 11, 115003 (2014) [arXiv:1403.4736 [hep-ph]].
- [45] P. M. Ferreira, R. Guedes, M. O. P. Sampaio and R. Santos, JHEP **1412**, 067 (2014) [arXiv:1409.6723 [hep-ph]].
- [46] D. Eriksson, J. Rathsmann and O. Stal, Comput. Phys. Commun. **181**, 189 (2010) [arXiv:0902.0851 [hep-ph]].

- [47] N. G. Deshpande and E. Ma, Phys. Rev. D **18**, 2574 (1978).
- [48] P. M. Ferreira, R. Santos and A. Barroso, Phys. Lett. B **603**, 219 (2004) [Erratum: Phys. Lett. B **629**, 114 (2005)] [hep-ph/0406231].
- [49] A. Barroso, P. M. Ferreira, I. P. Ivanov and R. Santos, JHEP **1306**, 045 (2013) [arXiv:1303.5098 [hep-ph]].
- [50] A. G. Akeroyd, A. Arhrib and E. M. Naimi, Phys. Lett. B **490**, 119 (2000) [hep-ph/0006035].
S. Kanemura, T. Kubota and E. Takasugi, Phys. Lett. B **313**, 155 (1993) [hep-ph/9303263].
- [51] S. Kanemura, M. Kikuchi and K. Yagyu, Nucl. Phys. B **896**, 80 (2015) [arXiv:1502.07716 [hep-ph]].
- [52] M. Baak *et al.* [Gfitter Group], Eur. Phys. J. C **74**, 3046 (2014) [arXiv:1407.3792 [hep-ph]].
- [53] P. Bechtle, O. Brein, S. Heinemeyer, G. Weiglein and K. E. Williams, Comput. Phys. Commun. **181**, 138 (2010) [arXiv:0811.4169 [hep-ph]].
- [54] P. Bechtle, O. Brein, S. Heinemeyer, G. Weiglein and K. E. Williams, Comput. Phys. Commun. **182**, 2605 (2011) [arXiv:1102.1898 [hep-ph]].
- [55] P. Bechtle, O. Brein, S. Heinemeyer, O. Stl, T. Stefaniak, G. Weiglein and K. E. Williams, Eur. Phys. J. C **74**, no. 3, 2693 (2014) [arXiv:1311.0055 [hep-ph]].
- [56] P. Bechtle, S. Heinemeyer, O. Stal, T. Stefaniak and G. Weiglein, Eur. Phys. J. C **75**, no. 9, 421 (2015) [arXiv:1507.06706 [hep-ph]].
- [57] P. Bechtle, S. Heinemeyer, O. Stl, T. Stefaniak and G. Weiglein, Eur. Phys. J. C **74**, no. 2, 2711 (2014) [arXiv:1305.1933 [hep-ph]].
- [58] M. Aaboud *et al.* [ATLAS Collaboration], arXiv:1709.07242 [hep-ex].
- [59] A. M. Sirunyan *et al.* [CMS Collaboration], arXiv:1803.06553 [hep-ex].
- [60] CMS Collaboration [CMS Collaboration], CMS-PAS-HIG-14-029.
- [61] G. Aad *et al.* [ATLAS Collaboration], Eur. Phys. J. C **76** no.1, 45 (2016) [arXiv:1507.05930 [hep-ex]].
- [62] M. Aaboud *et al.* [ATLAS Collaboration], Eur. Phys. J. C **78**, no. 4, 293 (2018) [arXiv:1712.06386 [hep-ex]].
- [63] V. Khachatryan *et al.* [CMS Collaboration], JHEP **1510**, 144 (2015) [arXiv:1504.00936 [hep-ex]].
- [64] A. M. Sirunyan *et al.* [CMS Collaboration], JHEP **1806**, 127 (2018) [arXiv:1804.01939 [hep-ex]].
- [65] G. Aad *et al.* [ATLAS Collaboration], Phys. Rev. D **92**, 092004 (2015) [arXiv:1509.04670 [hep-ex]].
- [66] A. M. Sirunyan *et al.* [CMS Collaboration], Phys. Lett. B **778**, 101 (2018) [arXiv:1707.02909 [hep-ex]].
- [67] A. M. Sirunyan *et al.* [CMS Collaboration], JHEP **1801**, 054 (2018) [arXiv:1708.04188 [hep-ex]].
- [68] G. Aad *et al.* [ATLAS Collaboration], Eur. Phys. J. C **76**, no. 4, 210 (2016) [arXiv:1509.05051 [hep-ex]].
- [69] V. Khachatryan *et al.* [CMS Collaboration], JHEP **1710**, 076 (2017) [arXiv:1701.02032 [hep-ex]].
- [70] G. Aad *et al.* [ATLAS Collaboration], Phys. Lett. B **744**, 163 (2015) [arXiv:1502.04478 [hep-ex]].
- [71] V. Khachatryan *et al.* [CMS Collaboration], Phys. Lett. B **748**, 221 (2015) [arXiv:1504.04710 [hep-ex]].

- [72] M. Aaboud *et al.* [ATLAS Collaboration], JHEP **1809**, 139 (2018) [arXiv:1807.07915 [hep-ex]].
- [73] G. Aad *et al.* [ATLAS Collaboration], JHEP **1603**, 127 (2016) [arXiv:1512.03704 [hep-ex]].
- [74] G. Aad *et al.* [ATLAS and CMS Collaborations], JHEP **1608**, 045 (2016) [arXiv:1606.02266 [hep-ex]].
- [75] The ATLAS collaboration [ATLAS Collaboration], ATLAS-CONF-2016-112.
- [76] The ATLAS collaboration [ATLAS Collaboration], ATLAS-CONF-2018-004.
- [77] M. Aaboud *et al.* [ATLAS Collaboration], JHEP **1712**, 024 (2017) [arXiv:1708.03299 [hep-ex]].
- [78] M. Aaboud *et al.* [ATLAS Collaboration], JHEP **1803**, 095 (2018) [arXiv:1712.02304 [hep-ex]].
- [79] M. Aaboud *et al.* [ATLAS Collaboration], Phys. Rev. D **97**, no. 7, 072003 (2018) [arXiv:1712.08891 [hep-ex]].
- [80] M. Aaboud *et al.* [ATLAS Collaboration], Phys. Rev. D **97**, no. 7, 072016 (2018) [arXiv:1712.08895 [hep-ex]].
- [81] M. Aaboud *et al.* [ATLAS Collaboration], arXiv:1802.04146 [hep-ex].
- [82] CMS Collaboration [CMS Collaboration], CMS-PAS-HIG-16-040.
- [83] A. M. Sirunyan *et al.* [CMS Collaboration], JHEP **1711**, 047 (2017) [arXiv:1706.09936 [hep-ex]].
- [84] A. M. Sirunyan *et al.* [CMS Collaboration], Phys. Lett. B **779**, 283 (2018) [arXiv:1708.00373 [hep-ex]].
- [85] A. M. Sirunyan *et al.* [CMS Collaboration], Phys. Rev. Lett. **120**, no. 7, 071802 (2018) [arXiv:1709.05543 [hep-ex]].
- [86] A. M. Sirunyan *et al.* [CMS Collaboration], Phys. Lett. B **780**, 501 (2018) [arXiv:1709.07497 [hep-ex]].
- [87] A. M. Sirunyan *et al.* [CMS Collaboration], JHEP **1808**, 066 (2018) [arXiv:1803.05485 [hep-ex]].
- [88] A. M. Sirunyan *et al.* [CMS Collaboration], JHEP **1806**, 101 (2018) [arXiv:1803.06986 [hep-ex]].
- [89] A. M. Sirunyan *et al.* [CMS Collaboration], arXiv:1804.03682 [hep-ex].
- [90] A. M. Sirunyan *et al.* [CMS Collaboration], [arXiv:1806.05246 [hep-ex]].
- [91] A. M. Sirunyan *et al.* [CMS Collaboration], Eur. Phys. J. C **77**, no. 10, 710 (2017) [arXiv:1705.04650 [hep-ex]].
- [92] A. M. Sirunyan *et al.* [CMS Collaboration], JHEP **1805**, 025 (2018) [arXiv:1802.02110 [hep-ex]].
- [93] M. Aaboud *et al.* [ATLAS Collaboration], Eur. Phys. J. C **77**, no. 12, 898 (2017) [arXiv:1708.03247 [hep-ex]].
- [94] M. Aaboud *et al.* [ATLAS Collaboration], JHEP **1712**, 085 (2017) [arXiv:1709.04183 [hep-ex]].
- [95] M. Aaboud *et al.* [ATLAS Collaboration], JHEP **1806**, 108 (2018) [arXiv:1711.11520 [hep-ex]].
- [96] A. M. Sirunyan *et al.* [CMS Collaboration], JHEP **1710**, 019 (2017) [arXiv:1706.04402 [hep-ex]].
- [97] A. M. Sirunyan *et al.* [CMS Collaboration], JHEP **1710**, 005 (2017) [arXiv:1707.03316 [hep-ex]].
- [98] A. M. Sirunyan *et al.* [CMS Collaboration], Phys. Rev. D **97**, no. 3, 032009 (2018) [arXiv:1711.00752 [hep-ex]].

- [99] M. Aaboud *et al.* [ATLAS Collaboration], JHEP **1801**, 126 (2018) [arXiv:1711.03301 [hep-ex]].
- [100] M. Aaboud *et al.* [ATLAS Collaboration], JHEP **1709**, 084 (2017) [arXiv:1706.03731 [hep-ex]].
- [101] M. Aaboud *et al.* [ATLAS Collaboration], JHEP **1711**, 195 (2017) [arXiv:1708.09266 [hep-ex]].
- [102] M. Aaboud *et al.* [ATLAS Collaboration], Phys. Rev. D **96**, no. 11, 112010 (2017) [arXiv:1708.08232 [hep-ex]].
- [103] M. Aaboud *et al.* [ATLAS Collaboration], Phys. Rev. D **97**, no. 11, 112001 (2018) [arXiv:1712.02332 [hep-ex]].
- [104] A. M. Sirunyan *et al.* [CMS Collaboration], Phys. Rev. D **96**, no. 3, 032003 (2017) [arXiv:1704.07781 [hep-ex]].
- [105] Y. Amhis *et al.* [Heavy Flavor Averaging Group (HFAG)], arXiv:1412.7515 [hep-ex].
- [106] F. Archilli, arXiv:1411.4964 [hep-ex].
- [107] K. A. Olive *et al.* [Particle Data Group], Chin. Phys. C **38**, 090001 (2014).
- [108] F. Gianotti *et al.*, Eur. Phys. J. C **39**, 293 (2005) [hep-ph/0204087].
- [109] F. Mahmoudi, Comput. Phys. Commun. **180**, 1579 (2009) [arXiv:0808.3144 [hep-ph]].
- [110] A. Arhrib, R. Benbrik, S. Moretti, R. Santos and P. Sharma, Phys. Rev. D **97** (2018) no.7, 075037 [arXiv:1712.05018 [hep-ph]].